Universidade de Lisboa

Faculdade de Farmácia

Development of scaffold based on electrospinning fiber for tendon and ligament reparation

Ana Raquel Gonçalves Heleno

Mestrado Integrado em Ciências Farmacêuticas

2019

Universidade de Lisboa

Faculdade de Farmácia

Development of scaffold based on electrospinning fiber for tendon and ligament reparation

Ana Raquel Gonçalves Heleno

Monografia do Mestrado Integrado em Ciências Farmacêuticas apresentada à Universidade de Lisboa através da Faculdade de Farmácia

Orientador: Prof. Dra. Giuseppina Sandri

Co-orientador: Prof. Dra. Maria Henriques Ribeiro, Professora Associada

2019

Este trabalho foi realizado durante o período de intercâmbio ao abrigo do programa Erasmus+, realizado no Dipartimento di Scienze del Farmaco da Universitá Degli Studi Di Pavia (UNIPV), em Itália.

Università degli Studi di Pavia

Resumo

Os Tendões são estruturas anatómicas interpostas entre músculos e ossos, cuja função é transmitir a força criada no músculo para osso, possibilitando o movimento e permitindo a manutenção da postura corporal. Quando um tendão está lesionado, a sua estrutura é afetada. Os tendões têm uma capacidade reparadora basal, mas quando são sobrecarregados por processos repetitivos levam a traumas relevantes.

A engenharia de tecidos visa regenerar tecidos danificados em vez de substituí-los, desenvolvendo substitutos biológicos, que são estruturas poliméricas capazes de simular as características da matriz extracelular e atuar como suporte para o crescimento de tecidos, ajudando a adesão, migração, proliferação e diferenciação dos tecidos. Membranas nanofibrosas eletrofiadas foram desenvolvidas, com uma morfologia homogénea tornando-as substratos ideais para o crescimento celular e para a regeneração tecidual.

A fabricação de nanofibras poliméricas por eletrospinning tem recebido mais atenção nos últimos anos, porque é uma técnica simples e versátil para com materiais poliméricos ou cerâmicos permitir a criação de fibras de tamanho milimétrico. O processo de eletrospinning rege-se por muitos parâmetros que podem ser classificados em parâmetros da solução (concentração da solução, peso molecular do polímero, viscosidade da solução, tensão superficial, condutividade), parâmetros do processo (campo elétrico, tipos de coletores, distância entre a ponta da seringa e o coletor) e parâmetros ambientais (humidade, temperatura).

As propriedades mecânicas das nanofibras podem ser controladas através da alteração dos parâmetros de eletrospinning, depende da sua composição química, do processo de fabricação, do diâmetro das fibras e do seu alinhamento.

As nanofibras poliméricas têm propriedades diferentes que as tornam favoráveis para muitas aplicações. Com base nisso, os scaffolds nanofibrosos representam um ambiente melhor para a ligação, proliferação e função.

O objetivo deste estudo foi preparar scaffolds 3D nanofibrosos contendo hidroxiapatite. A composição considerada foi baseada em pululano, quitosano, ácido cítrico e ácido acético. Foram utilizadas duas concentrações diferentes de hidroxiapatite, juntando aos polímeros para obter scaffolds com hidroxiapatite.

Palavras-chave: Tendões, Hidroxiapatite, Scaffolds, Electrospinning, Engenharia de tecidos

Abstract

Tendons are anatomic structures interposed between muscles and bones, whose function is to transmit the force created in the muscle to bone, making joint movement possible and allowing the maintenance of body posture. When a tendon is injured, its structure is disarranged. Tendons have a basal reparative ability, but when they are overwhelmed by repetitive and traumatic processes, it causes damage.

Tissue engineering aims to regenerate damaged tissues instead of replacing them, by developing biological substitutes, which are polymeric scaffolds able to simulate the characteristics of the extracellular matrix and to act as a support for tissue growth encouraging the adhesion, migration, proliferation and differentiation of the cells. Electrospun nanofibrous membranes have been developed, which have a homogeneous morphology that makes them ideal substrates for cell growth and tissue regeneration.

The manufacturing of polymeric nanofibers by electrospinning has received much attention in recent years, because is a simple and versatile technique for spinning polymeric or ceramic materials that allows the creation of sub-millimeter-sized fibres. The electrospinning process is governed by many parameters that can be classified into solution parameters (concentration of the solution, molecular weight of the polymer, solution viscosity, surface tension, conductivity), process parameters (electric field, types of collectors, distance between the tip and the collector) and ambient parameters (humidity, temperature).

The mechanical properties of nanofibers can be controlled by manipulating the electrospinning parameters, it depends on their chemical composition, on the fabrication procedure, the fibres diameter and their alignment.

Polymeric nanofibers have different properties that make them favorable for many applications such as greater mechanical properties than larger fibres. Based on this, nanofibrous scaffolds represents a better environment for the binding, proliferation and functionality.

The purpose of this study was to prepare nanofibrous 3D scaffolds containing hydroxyapatite. The composition considered was based on pullulan, chitosan, citric acid and acetic acid. Two different concentrations of hydroxyapatite were used, by mixing into the polymer blends to obtain HAp-loaded scaffolds.

Key words: Tendons, Hydroxyapatite, Scaffolds, Electrospinning, Tissue engineering

Acknowledgements

A elaboração deste trabalho não teria sido possível sem o estímulo e colaboração de várias pessoas. Assim, gostaria de expressar a minha gratidão a todos aqueles que contribuíram para que este trabalho se tornasse realidade.

Obrigada aos professores que fizeram parte desta minha jornada na FFUL e na Faculdade de Farmácia de Pavia, como tal agradeço a orientação da professora Maria Henriques Ribeiro e da professora Giuseppina Sandri.

Obrigada a toda a equipa do laboratório do Dipartimento di Scienze del Farmaco da UNIPV que foram como uma família para mim e que tão bem me souberam acolher em Pavia sempre com boa disposição.

Obrigada aos meus pais, António Heleno e Anabela Heleno, por todo o apoio e presença nos momentos mais complicados e por serem a prova de que o amor nunca falha.

Obrigada ao meu irmão Tiago Heleno, porque apesar de tudo sei que está lá sempre para mim, tenho muito orgulho em nós.

Obrigada à minha avó Maria por estar sempre comigo em tudo e por ser a pessoa tão especial que é.

Obrigada ao meu avô António, pela paciência, por me ter ensinado a andar de bicicleta no Baleal, por me ter ensinado tudo sobre os planetas no baloiço que me fez na árvore da quinta, por ter feito de mim a criança mais feliz do mundo e por me ter ensinado que a saudade é a prova de que o passado valeu a pena.

Obrigada aos meus amigos, Ana Nunes, Joana Guerra, Cláudia Inácio, Cláudia Afonso, Rodrigo Borrega, Luís Pinheiro, André Oliveira, João Soares, Ana Patrícia Gomes, Ariana Oliveira, Inês Paulo, Joana Amaral por toda a amizade e companheirismo ao longo deste percurso e de mais uma etapa que está a chegar ao fim.

Abreviaturas

EBA	European Bioplastic Association
ECM	Extracellular matrix
GAGs	Glycosaminoglycans
HAp	Hydroxyapatite
MTJ	Myotendinous junction
OTJ	Osteotendinous junction
PGs	Proteoglycans
PRP	Platelet rich plasma
TSCs	Tendon stem/progenitor cells

Table of contents

1 Introduction 13
1.1 Tendons 13
1.1.1 Structure and metabolism of tendons 13
1.1.2 Tendons microscopic anatomy 14
1.1.2.1 Cellular component 14
1.1.2.2. The extracellular matrix (ECM) 14
1.1.3 Mechanical properties of tendons 15
1.1.3.1 The stress strain curve 15
1.2 Tendinopathy 16
1.2.1. Etiology 16
1.2.2. Anatomical mechanism of injury and repair 16
1.3. Traditional approaches for the treatment of injuries 16
1.4. Regenerative Medicine Approaches 17
1.4.1. Cell-based therapy 17
1.4.2. Scaffolds for tendon regeneration 17
1.4.2.1 Scaffolds requirements 17
1.4.2.2. Polymeric nanofibers obtained through electrospinning 18
1.4.2.3 Electrospinning 18
1.4.2.3.1. Parameters influencing the electrospinning 19
1.4.2.4. Biopolymers for the production of nanofibers scaffolds 21
1.4.2.4.1 Chitosan 21
1.4.2.4.2. Pullulan 22
1.5. Bone tissue 22
1.5.1 Hydroxyapatite 23
1.5.2. Structure and properties of hydroxyapatite 23
1.5.3. Hydroxyapatite solubility 25
1.5.4. Biological and synthetic hydroxyapatite 25
1.5.5. Biomedical use 26
2 Objective 27
3 Materials 28
4 Methods 29
4.1 Preparation of polymeric solutions 29
4.2 Characterization of the polymeric solutions 29

4.2.1 Measurement of consistency 29
4.2.2 Surface tension 30
4.2.3 Conductivity 30
4.2.4 X-ray diffraction 30
4.3 Electrospinning (polymeric solutions) 30
4.3.1 Nanofibers cross linking process 32
4.4 Characterization of the nanofibers 32
4.4.1 Solubility test 32
4.4.2 Scanning Electron Microscope (SEM) 32
4.4.3 Transmission Electron Microscope (TEM) 32
4.4.4 Contact angle 33
4.4.5 FT-IR Spectroscopy 33
4.4.6 Analysis of the mechanical properties 34
5 Results and discussion 36
5.1 Characterization of the polymeric solutions 36
5.1.1 Consistency 36
5.1.2 Surface tension 36
5.1.3 Conductivity 37
5.1.4 X-ray diffraction 37
5.1.5 Scanning Electron Microscope (SEM) 37
5.2 Morphological characterization 38
5.2.1 Scanning Electron Microscope (SEM) 38
5.2.2 Transmission Electron Microscope (TEM) 40
5.2.3 Wettability evaluation 40
5.2.4 FT-IR analysis 41
5.2.5 Tensile measures and evaluation of the mechanical properties 42
5.2.5.1 Tensile measures on fibres randomly oriented 42
5.2.5.2 Tensile measures on closed tubular scaffolds in aligned orientation 43
6 Conclusion and future perspectives 47
7 References 48

List of Figures:

Figure 1 The organization of tendon structure (1) 13

Figure 2 The extracellular matrix components (5) 14

Figure 3 The stress-strain curve of the tendon (10) 15

Figure 4 Functioning scheme of electrospinning. (22) 19

Figure 5 Scheme of an electrospinning with a static collector (a) and a rotating collector (b) (22) 21

Figure 6 Chitin and Chitosan structure (29) 21

Figure 7 Chemical structure of pullupan (35) 22

Figure 8 Hierarchical structural organization of bone: cortical and cancellous bone; osteons with Haversian systems; lamellae; collagen fiber assemblies of collagen fibrils; bone mineral crystals, collagen molecules, and non-collagenous proteins. (41) 23

Figure 9 Projection of the constituting ions of HAp on the basal (001) plane 24

Figure 10 Electrospinning STKIT-40 Linari Engineering with a static collector (a) and a rotating collector (b) 31

Figure 11 Nanofibers electrospun in tubular conformation with a rotating collector of inox steel 32

Figure 12 Contact angle of a water drop with a solid surface; <90° indicates wetting (a) and ≥90° indicates nonwetting (b). (63) 33

Figure 13 TA.XT plus Texture Analyser (ENCO, Spinea I) equipped with two clamps for the fibres mechanical properties analysis 34

Figure 14 Penetration profiles evaluated for F1 (polymeric blend based on PLL and CH), F2 and F3 (polymeric blend having the same composition as F1, but containing hydroxyapatite HAp at 0,1% or 0,5% w/w) 36

Figure 15 Values of surface tension (mN/m) evaluated for F1 (polymeric blend based on PLL and CH), F2 and F3 (polymeric blend having the same composition as F1, but containing hydroxyapatite HAp at 0,1% or 0,5% w/w) 36

Figure 16 Values of conductivity (µS/cm) evaluated for F1 (polymeric blend based on PLL and CH), F2 and F3 (polymeric blend having the same composition as F1, but containing hydroxyapatite HAp at 0,1% or 0,5% w/w) 37

Figure 17 X-ray diffraction of the HAp powder (200 nm) compared with the HAp 0,1% in water and with the HAp 0,1% in acetic acid 37

Figure 18 SEM images of the F2 formulation (HAp 0,1%) without polymer compared with a solution of water with the 0,1% of HAp at two different magnifications (100 kx and 50.0 kx) 38

Figure 19 SEM images of the F1, F2 and F3 formulations randomly collected at two different magnifications (10.0 kx and 2.00 kx) 38

Figure 20 SEM images of the aligned F1, F2 and F3 nanofiber-based scaffolds reinforced with F4 and F5 at two different magnifications (10.0 kx and 2.00 kx), collected with 3 mm drum 39

Figure 21 SEM images of the aligned F2 and F3 scaffolds, reinforced with F5 after 6 days of hydration, at two different magnifications (10.0 kx and 2.00 kx) 40

Figure 22 TEM images of the F1 and F2 formulations at two different magnifications (15k and 50k) 40

Figure 23 Values of the contact angle (deg) of F1, F2 and F3 scaffolds randomly collected . 41

Figure 24 FT-IR spectra of the hydroxyapatite powder (64) 41

Figure 25 FT-IR profiles of the F1, F2 and F3 scaffolds randomly collected and after crosslinking 42

Figure 26 Stress-strain curves evaluated for F1, F2 and F3 formulations both in dry (a) and hydrated (b) state randomly oriented, prepared with a static collector 42

Figure 27 Maximum tensile force values (mN/mm2) evaluated for F1, F2 and F3 formulations both in dry (a) and hydrated (b) state randomly oriented, prepared with a static collector 43

Figure 28 Elongation (%) values evaluated for F1, F2 and F3 formulations both in dry (a) and hydrated (b) state randomly oriented, prepared with a static collector 43

Figure 29 Young Modulus (mN/mm2) values evaluated for F1, F2 and F3 formulations both in dry (a) and hydrated (b) state randomly oriented, prepared with a static collector..... 43

Figure 30 Stress-strain curves of the F1, F2 and F3 formulations reinforced with F4 and F5 as inner layer, both in dry (a) and hydrated (b) state, evaluated for the closed aligned scaffolds prepared with a rotating collector having the diameter of 0,8mm 44

Figure 31 Stress-strain curves of the F1, F2 and F3 formulations reinforced with F4 and F5 as inner layer, both in dry (a) and hydrated (b) state, evaluated for the closed aligned scaffolds prepared with a rotating collector having the diameter of 3mm 44

Figure 32 Direct comparison of maximum tensile force (mN/mm2), both in dry (a) and hydrated (b) state, for the scaffolds randomly collected and for the aligned 3D scaffolds, reinforced with F4 and F5 as inner layer 45

Figure 33 Direct comparison of elongation (%), both in dry (a) and hydrated (b) state, for the scaffolds randomly collected and for the aligned 3D scaffolds, reinforced with F4 and F5 as inner layer 45

Figure 34 Direct comparison of Young modulus (mN/mm2), both in dry (a) and hydrated (b) state, for the scaffolds randomly collected and for the aligned 3D scaffolds, reinforced with F4 and F5 as inner layer 46

List of tables:

Table 1 Mechanical properties of hydroxyapatite (52) 24

Table 2 Qualitative and quantitative composition of the solutions 29

Table 3 Qualitative and quantitative composition of the solutions 29

Table 4 Electrospinning parameters of the solutions in Table 2 and 3 31

Table 5 Dimensions of the fibre pieces for the analysis of the mechanical properties 34

1 Introduction

1.1 Tendons

Tendons and ligaments are connective tissues that guide motion, share loads, and transmit forces in a manner that is unique to each as well as the anatomical site and biomechanical stresses to which they are subjected. Tendons are anatomic structures interposed between muscles and bones, with a predominantly mechanical function: translating muscular contractions into joint movement by transmitting forces from muscle to bone allowing the maintenance of body posture. Because its stiffness is intermediate between that of muscle and that of bone, tendon acts as a buffer to prevent stress concentrations that would result from a direct muscle-to-bone connection. (1) (2)

Healthy tendons have a fibro-elastic texture that shows a great resistance to mechanical loads with minimal deformations. They appear white because they are relatively avascular, they are made up of 30% collagen and 2% elastin in an extracellular matrix, which is formed by 68% of water. Elastin contributes to the flexibility of the tendon, while collagen is responsible for the resistance.

Each muscle has two tendons, proximal and distal. The point of union with a muscle is called an MTJ, while the point of union with a bone is called an OTJ. (3)

1.1.1 Structure and metabolism of tendons

Tendons are hierarchical structures composed primarily of collagen fibrils. Triple helical collagen molecules assemble to form fibrils. Fibrils bunble together to form fibers. Within the mature tendon, fibers are grouped together with tenocytes within fascicles that are surrounded by a cellular, loose connective tissue, the endotenon. (fig.1.) (1) A collagen fiber is the smallest unit of tendons visible using light microscopy and it's also the smallest collagenous structure that can be mechanically tested. Tendons consist of closely packed of collagen fibres, parallel to one another, so they can ensure an optimal resistance to mechanical stresses.

Regarding the metabolism, tendons are metabolically active and they work like all other collagen-based structures. The metabolism of collagen in tendons is relatively slow with a balance between synthesis and breakdown, and it's normally increased after an injury or exercise. (2)

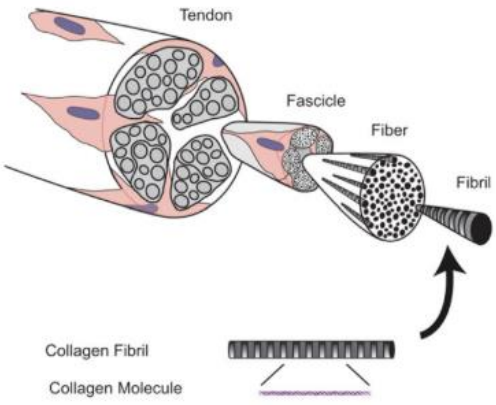

Figure 1 The organization of tendon structure (1)

1.1.2 Tendons microscopic anatomy

Tendons are composed mainly of collagen fibres and elongated fibroblast-like cells within an extracellular matrix (4)

1.1.2.1 Cellular component

Cellular component is composed by fibroblast-like cells, the tenocytes. Tenocytes are fusiform cells that are arranged in lines on the collagen fibres that synthesize the collagen, and they contribute to the maintenance of the macromolecular components that compose the ECM. There's a small number of tenocytes in the tendon and that is why there's a low cellular turnover, leading to poor healing abilities of tendons. (5)

1.1.2.2. The extracellular matrix (ECM)

The extracellular tendon matrix is composed by the collagen fibres, elastic fibres, the ground substance and the inorganic components (Fig. 2). Tendons are mostly composed by type I collagen, but they contain some of other types too (II, III, IV, V, VI). For example, type II and type III are the main components of the paratenon. Collagen fibres are oriented longitudinally, transversely and horizontally, forming spirals and plaits; this complex structure gives the tendons an higher resistance to tensile. Elastic fibres are just the 1-2% of the dry mass of the tendon. The ground substance surrounds the collagen and it's composed by PGs, GAGs, structural glycoproteins and other small molecules. Particularly the PGs and the GAGs have a high water-binding capacity, that improves the biomechanical properties of tendons, such as elasticity against compressive forces. They confer on tendons the high capacity to withstand the forces because of their rigidity, due to the charge-to-charge repulsion forces and their high charge density. Inorganic components are less of the 0,2% of the tendon dry mass. The component in higher concentrations is calcium (for development of the osteotendinous junction), magnesium, cobalt, zinc, copper, manganese, nickel, cadmium, lithium, fluoride, lead, silicon and phosphor, they are involved in growth, development and normal metabolism of the musculoskeletal structures. (3)

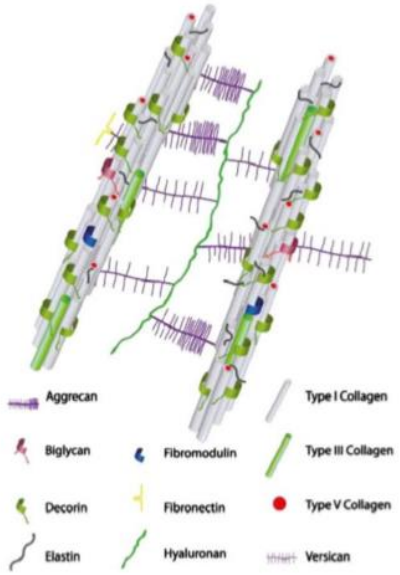

Figure 2 The extracellular matrix components (5)

1.1.3 Mechanical properties of tendons

The function of tendons is to transmit the mechanical impulses created during the muscle's contensile to bone. (3)

Tendons are viscoelastic, because of the collagen fibres and elastin, and they have a time dependent behaviour. Their viscoelasticity is not linear and it's characterized by a Young's modulus (that is the slope of the stress-strain curve) that increases from small values at small strains to high values at higher strains. A short tendon has more resistance to tensile than a long tendon, because it needs a more intense load to break, but a long tendon has an enhanced ability of deformation before the break. (6)

The mechanical properties of tendons are related to the collagen fibrils diameter: fibrils with a small diameter are elastic and they have more resistance to the plastic flow, because of their surface area and their greater potential of connections, while fibrils with a large diameter are stronger and more resistant to tensile force, because they have a greater density of intramolecular cross-links. The tendon needs for both smaller and larger fibrils to have both resistance to tensile force that resistance to the plastic flow. (7)

1.1.3.1 The stress strain curve

The mechanical behaviour includes the manner in which a material is deformed and reaches the break when subjected to outside forces. The tendon has three distinct fundamental properties: Elasticity, plasticity and viscosity.

The stress-strain curve (Fig.3.) shows the mechanical behaviour of the tendon at different stress levels and it can be divided into three different phases. The initial region of the curve is the toe region, it shows that the stress increases with the strain until a constant value and it corresponds to the straightening of the crimped fibres, the fibres are aligned in the direction of the load and respond directly to the strain. Next is the heel region, in which the extension of the fascicles also requires the sliding of collagen components, when strain increases the tissue rigidity increases and the tendon endures only small deformations (8) The third phase is the linear region and no further extension is possible, the break occurs when the intra- and intermolecular collagen bonds are broken. (9)

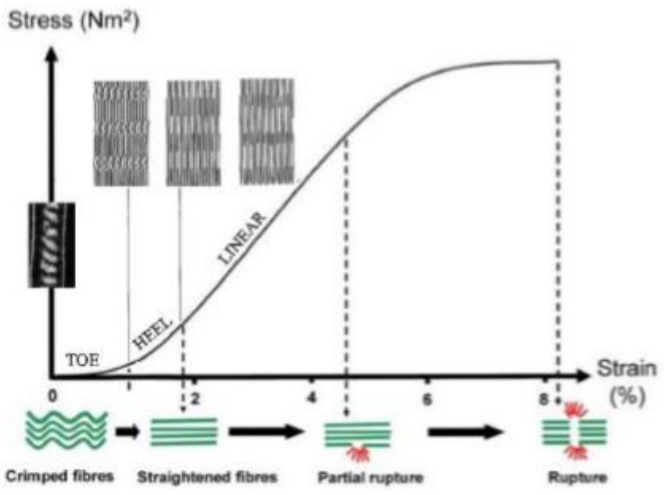

Figure 3 The stress-strain curve of the tendon (10)

1.2 Tendinopathy

The term tendinopathy refers to several diseases that affect the osteotendinous junction. (2) These diseases can affect the tendons (tendinitis), the synovial sheath, or the peritoneum or bursitis. Often all of these conditions are present simultaneously. Injury can appear at any point of the muscle-tendinous unit: in the tendon, in the muscle, or even at the musculotendinous junction and at the point of intersection to bone. The injury appears in the weakest point of the unit. Tendinopathies account for 30-50% of all sports injuries and their incidence has increased in recent decades due to population aging. (11) The condition can be significantly debilitating because it causes pain, loss of muscle function, joint instability and abnormal movements. It could also lead to secondary pathologies and all this negatively affects the patient's quality of life. (12)

1.2.1. Etiology

Most tendinopathies are not caused by a single factor, but there are several contributing elements that can be intrinsic and extrinsic factors. Physical training is an important factor in the onset of tendinopathies that occur mainly at an early age and in sportsmen. Injuries may be caused by direct trauma or repeated microtrauma. Healthy tendons when subjected to excessive tension are quite resilient, while the tendon weakened by continuous microtrauma has a gradually diminishing resistance, making it more susceptible to injury. Other factors that may be considered contributors in the establishment of tendinopathies are: endogenous factors, such as congenital anomalies and constitutional factors such as age, gender and tissue reactivity. (9)

1.2.2. Anatomical mechanism of injury and repair

With inactivity, the reabsorption of collagen is increased, so more collagen is laid down to provide more strength if necessary. But in the first phase of activity the collagen turnover is so rapid that the basal reparative processes are overwhelmed. (9) This is the period where the most common overuse injuries can occur. Mechanisms primarily responsible for the tendon injuries: tension, when applied quickly; tension, when applied obliquely; innervation, when it is at maximum levels in the attached muscle; the tendon is weak compared with the muscle. The highest frequency of failure corresponds to ages of more than 30 years, when tendons are more susceptible to injury due to a progressive deterioration of collagen. Elastin and proteoglycan matrix decrease and the water content decrease from 80% to 30%, this leads to less elasticity. (12)

1.3. Traditional approaches for the treatment of injuries

Nowadays for the tendon injuries two different kind of approaches are used: preservative, surgical or both. This type of treatment aims to eliminate pain, reduce inflammation and promote healing. Preservative approach, principally used in not serious cases, consists of: rest, exercises, drug therapy, ultrasound and laser. This recovery approach requires long periods of treatment, partial loss of function and recurrent lesions due to the limited capacity of self-healing of the tendon. In cases of total break, the surgical treatment is chosen, and it involves the suturing of the wounds or the fixation of the tendon to the bone and after that is essential to follow a rehabilitation program. Surgical repair techniques have been developed, through the

use of sutures and anchors to the soft tissue restoring the biomechanical properties of the tendon before the injury. (13)

1.4. Regenerative Medicine Approaches

In recent years, several studies have been conducted on the application of biological treatments or tissue engineering approaches to the treatment of tendon injuries. Regenerative medicine is subdivided into cell therapy, which does not use scaffolds, and in tissue engineering, which uses scaffolds as a support for regeneration. (13)

1.4.1. Cell-based therapy

Cell therapy is based on the use of cells capable of inducing synthesis of materials effective in the tendon healing process and consists of direct injection of cells into the damaged site. One of the biggest problems, is finding a sufficient number of authentic cells and an appropriate source for every patient. A vehicle capable of preventing cell membrane breakage during the injection process is required, facilitating cell survival and functionality. TSCs PRP hold great potential to effectively treat tendon injurie and are particularly effective in improving tendon structure and function. (14)

1.4.2. Scaffolds for tendon regeneration

With tissue engineering is possible to reconstruct damaged tissue, implant the cells in three-dimensional scaffolds that has functions similar to those of the extracellular matrix, allowing cell proliferation, differentiation and biosynthesis. These scaffolds essentially act as a model, recreating the spatial organization of the original tissue, providing a surface that facilitates adhesion, survival, migration, proliferation and differentiation of progenitor cells. Scaffolds can be grown in vitro or implanted directly at the damaged site using body systems in which tissue or organ regeneration is induced in vivo. (15)

Resorbable scaffolds have been developed to overcome the problems arising from fixed implantations. They are characterized by: rate of resorption, kinetics of loss of mechanical properties, nature and concentration of released products. In the first phase of the repair process, scaffolds should protect cells and new tissue from high strains, but allow for gradual exposure to loads in subsequent phases. Degradation products should not be harmful to surrounding tissues, induce chronic inflammation or other harmful biological response. (16)

1.4.2.1 Scaffolds requirements

Numerous scaffolds have been produced from a wide variety of biomaterials using various manufacturing techniques. Regardless of the tissue type, it is important to design suitable scaffolds that meets the following requirements:

- Biocompatibility: Cells must adhere, function normally, migrate to the surface, and finally through them, to begin proliferating. After implantation, these scaffolds should cause a negligible immune reaction to prevent the insurgence of a severe inflammatory response that may reduce healing or cause body rejection. (15)
- Biodegradation: Scaffolds must be biodegradable to allow cells to reproduce their own extracellular matrix. In addition, products resulting from this degradation must also be non-toxic and able to escape the body without causing interference with other organs. (15)

- Mechanical properties: It is one of the greater challenges in tissue engineering. Ideally, a scaffold should exhibit mechanical properties consistent with the anatomical site in which it will be implanted and should be strong enough to allow surgical manipulation during implantation. (15)
- Scaffold architecture: Scaffolds should have a structure characterized by high porosity, with interconnected pores, to ensure cell penetration and proper nutrient diffusion into cells within the construct and extracellular matrix formed by these cells. Also, the average pore size is important. Pores must be large enough to allow cells to migrate to the structure, but small enough to establish a high specific surface to determine the minimum binder density capable of efficiently attaching cells to scaffolds. (15)
- Biomaterials: The main biomaterials used for scaffolds and tissue engineering are the ceramics, the synthetic polymers and the natural polymers. (15)

1.4.2.2. Polymeric nanofibers obtained through electrospinning

The manufacturing of polymeric nanofibers by electrospinning has received much attention in recent years. Polymeric nanofibers have different properties that make them favorable for many applications such as greater mechanical properties than larger fibres. (17) Based on this, nanofibrous scaffolds represents a better environment for the binding, proliferation and functionality; potential applications for these nanofibers include: tissue engineering scaffolds, filtration devices, sensors, materials development and electronic applications. (18)

Electrospinning is a method that leads to generate porous nanofibers, using a high voltage electrostatic field. The scaffold should have morphological similarity to the ECM of natural tissue, characterized by high porosity and efficient mechanical properties. (19) The ECM represents the natural three-dimensional microenvironment of cells, composed of fiber-forming proteins such as collagen and elastic fibers, as well as non-fiber-forming proteins such as proteoglycans, glycosaminoglycans and soluble factors. ECM is highly heterogeneous. The cells bind the receptors via surface cell receptors to the ECM, and this leads to activation of cellular responses such as migration, proliferation and differentiation. (20)

The mechanical properties of nanofibers can be controlled by manipulating the electrospinning parameters, it depends on their chemical composition, on the fabrication procedure, the fibres diameter and their alignment. (21)

1.4.2.3 Electrospinning

Over the last few years, the process of electrospinning has gained considerable attention mainly due to the growing interest in nanotechnologies, as the process allows the manufacture of ultra-thin fibres or fibrous structures composed of various polymers, with diameters in the order of sub micrometers or nanometers. Electrospinning is a simple and versatile technique for spinning polymeric or ceramic materials that allows the creation of sub-millimeter-sized fibers (from 2 nm to a few micrometers) by stretching a solution or a viscoelastic axis. In this technique, a wide variety of materials are used. There are currently two different standard configurations, vertical and horizontal. Electrospinning is performed at room temperature under atmospheric conditions. (22)

The basic experimental set up for electrospinning includes (Fig.4.): a syringe; a spinneret (usually a needle or a capillary tube); a syringe pump; a high voltage power supply (in the order of kV); a collector, that is a conductive flat or rotating electrode.

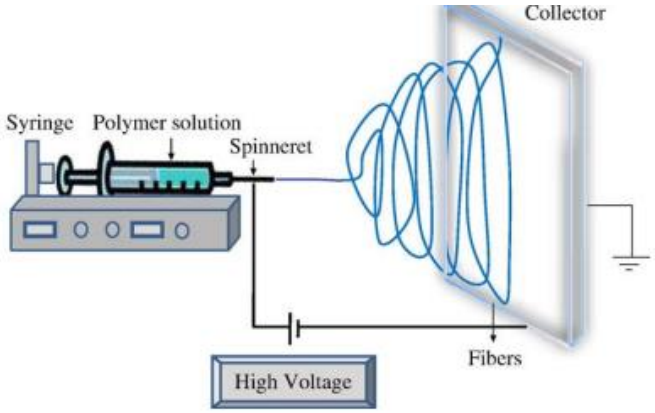

Figure 4 Functioning scheme of electrospinning. (22)

The syringe is connected to the syringe pump, the collector and the high voltage power supply. The polymeric fluid is introduced into the syringe into the capillary tube and, forms a droplet on the needle tip. The electric field to which the polymer solution is subjected is generated by applying a potential difference between the capillary and the collector in the order of tens of kV. The charges present in the solution are transferred to the surface, generating a repulsive force that opposes the surface tension of the liquid. Applying high voltage, the droplet adopts a conical shape, called "Taylor cone", and a thin fibre develops as soon as the electrical field strength exceeds the surface tension. The trajectory of the jet of solution expelled from the tip of the Taylor cone is controlled by the same electric field, and as the jet travels through the air, the solvent in the solution evaporates, leaving behind a dry fiber that deposits in the collector. (22)

Electrostatic repulsion leads to the formation of a long, thin and standard filament. Depending on the rheological properties of the solution and due to other spinning parameters, the resulting fibre diameter may range from tens of nanometers to a few micrometers. The main parameters that influence the morphology of electromagnetic fibers include viscosity, surface tension and solution´s density. Surface tension always tends to convert the liquid jet into one or more spherical droplets to minimize surface energy. Viscoelastic force also quickly resists shape changes. However, the relative intensities of these forces may change during the spinning process due to the lengthening of the jet and solvent evaporation. (23)

1.4.2.3.1. Parameters influencing the electrospinning

The electrospinning process is governed by many parameters that can be classified into solution parameters, process parameters and ambient parameters. Solution parameters include concentration of the solution, molecular weight of the polymer, solution viscosity, surface tension and conductivity; process parameters include applied electric field (the applied voltage), the flow rate of the polymer, types of collectors and the distance between the tip and the collector. Each of these parameters significantly affect the fibres morphology. (24) In addition to these variables, the ambient parameters consist of the humidity and temperature of the surroundings that affect the morphology and diameter of the elctrospun nanofibers. (22)

Solution parameters: The properties of the solution, such as viscosity, concentration, molecular weight, electrical conductivity, surface tension and solvent volatility, influence the nanofiber morphology. In the electrospinning process, for fibre formation to occur, a minimum solution concentration is required and, in addition, there is an ideal solution concentration in which the

fibres have the ideal characteristics. The ideal concentration value depends on the type of material used. When the optimal concentration is reached, smooth, compact and uniform nanofibers are collected. It has been shown that continuous and regular fibers cannot be obtained when the viscosity is very low and that with very high values it is difficult to have a continuous solution jet and in particular it is difficult to expel the jet from the syringe. Surface tension depends on the type of solvent used to prepare the solution and plays a critical role in the electrospinning process. Generally, the high surface tension of a solution inhibits the electrospinning process. Molecular weight also has a significant effect on rheological and electrical properties. The conductivity is determined by the polymer type and the solvent used and with its increase there is a decrease in the diameter of the nanofibers. Highly conductive solutions are unstable in the presence of strong electric fields and they form fibres with a small diameter. (22)

Processing parameters: In the electrospinning process a fundamental element is the applied voltage to the solution. When higher voltages are applied there is more polymer ejection and the formation of smaller fibres is facilitated. Indeed, an increase of the applied voltage increases the electrostatic repulsive forces on the fluid jet and causes a greater stretching of the solution, leading to rapid evaporation of solvent. At a higher voltage there is also a greater probability of beads formation, but the level of significance varies with the solution concentration and the distance between the tip and the collector. If the flow rate is too high, nanofibers will be produced with beads and thick diameters rather than uniform fine diameter nanofibers due to the short solvent evaporation time before reaching the collector and the low drawing forces. Finally, there is an ideal distance between the collector and the tip that allows to obtain uniform and dry nanofibers. If this distance is not respected and, in particular, is too short, the fiber will not have enough time to solidify before reaching the collector. (22)

Ambient parameters: Temperature and humidity influence the electrospinning process, since the average diameter of the produced nanofibers varies significantly after a change in these two parameters. It has been shown that a temperature increase favors the formation of fibers with a thinner diameter; this is due to the inverse relationship between temperature and viscosity. (25) Considerable variation in humidity is instead responsible for the different surface morphologies that the nanofiber membrane can support. At low relative humidity values, the solvent evaporates, fully accelerating the nanofiber drying process. (26) However, when the evaporation rate is much faster than the removal of solvent from the needle tip, electrophony continues for only a few minutes until the needle tip is blocked. (22)

Types of collectors: The electrospinning changes according to different types of collector used. The collector is the conductive substrate where the nanofibers are collected. The most used is the static collector with an aluminium foil (Fig.5 a), but it is adequate only for the production of fibres that are randomly oriented, while the aligned fibres need the rotating rod.(22) The nature of the collector influences significantly the morphological and physical properties of the spun fibres, The rotating drum collector (Fig.5 b) is the method commonly used to collect aligned arrays of fibres. The cylindrical drum is capable of rotating at high speeds (a few 1000 rpm). The alignment of the fibres is induced by the rotating drum and the degree of alignment improves with the rotational speed. At higher speeds the fibres obtained are highly aligned, due to a centrifugal force that is developed near the vicinity of the circumference of the rotating drum. However, at much higher speeds, the take-up velocity breaks the depositing fibre jet and continuous fibres are not collected. (27)

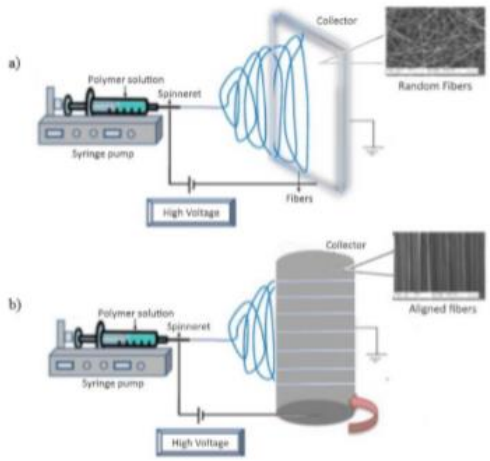

Figure 5 Scheme of an electrospinning with a static collector (a) and a rotating collector (b) (22)

1.4.2.4. Biopolymers for the production of nanofibers scaffolds

In the definition of biopolymers, as indicated by EBA, there are two types of macromolecules with different origins and characteristics: biodegradable polymers and polymers derived from renewable sources. The biodegradable polymers include chemical (redox reactions), physicochemical (photooxidation) or microbiological (enzymatic degradation). Polymers derived from renewable sources belong to those synthesized by living organisms. Biopolymers are capable of expressing various specific biological functions such as conservation and expression of genetic heritage, catalysis and regulation of metabolic reactions, protective and defensive action and communication with the external environment and with other microorganisms. Biopolymers play an important role in tissue repair and reconstruction processes and may be associated with other substances such as antimicrobials and growth factors. (28)

1.4.2.4.1 Chitosan

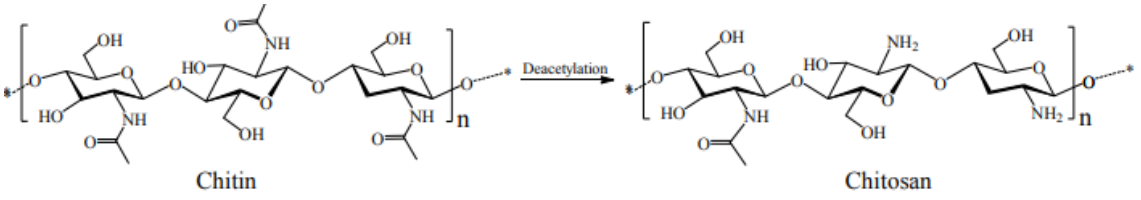

Figure 6 Chitin and Chitosan structure (29)

Chitosan (Fig. 6) is a linear polymer composed of D-glucosamine and N-acetyl-D-glucosamine, joined by β- (1 → 4) glycosidic bonds; It is obtained from a partial deacetylation of chitin, a natural biopolymer derived from the exoskeleton of crustaceans such as crabs, shrimps and lobsters. Chitosan is also found in some microorganisms such as yeast and fungi. (30)

Depending on the source and preparation procedure, the average molecular weight of chitosan may range from 50 to 1000 kDa, Chitosan is usually insoluble in aqueous solutions with pH greater than 7, while it is soluble in most organic acid solutions with pH below 6.5, including formic, acetic, tartaric and citric acid, while is insoluble in phosphoric and sulfuric acids. (31)

Chitosan has the particularity of interacting with different negatively charged molecules, such as proteins, anionic polysaccharides and fatty acids, capable of forming complexes with metals and surfactants. (32) In vitro and in vivo tests demonstrated the biocompatibility and biodegradability of this polymer. It is biocompatible because, in contact with biological systems, it does not cause toxic or harmful effects and does not trigger important immune or inflammatory responses, in fact, due to the presence of N-acetyl D-glucosamine, which interacts with different cell membrane receptors, is capable to modulate the immune response. It is biodegradable because it is degraded by endogenous enzymes such as glucosamine-glucosamine or glucosamine-N-acetyl glucosamine hydrolase, by lysozymes. (33)

Chitosan has remarkable pharmacological properties that offer great opportunities in the biomedical field. In fact, this polysaccharide exhibits antibacterial and antifungal activity against many pathogenic microorganisms, antioxidant activity against free radicals, hemostatic properties with dose dependent coagulation induction. In addition, it has mucoadhesive properties that make it a good promoter of drug absorption and also an excellent material for the production of scaffolds for tissue regeneration. This polymer can be biodegraded into non-toxic residues and the degradation rate is highly correlated with the polymer molecular weight and its degree of deacetylation. (34)

1.4.2.4.2. Pullulan

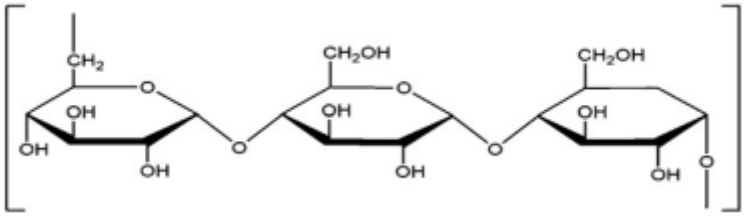

Figure 7 Chemical structure of pullupan (35)

Pullulan is a water-soluble polysaccharide produced aerobically by growing a yeast like fungus *Aureobasidium pullulans*. (36) Dry pullulan is white to off-white tasteless, odorless powder which forms a viscous non-hygroscopic solution when dissolved in water at 5–10%. As pullulan is highly water soluble so it can be used as a carrier for drug and it helps in controlled release of drug in plasma. Pullulan is biodegradable and has a considerable mechanical strength and other functional properties like adhesiveness, film formability, enzymatically mediated degradability. (35) It is neutral, non-toxic, non-immunogenic, non-cancerous. Therefore, it has been extensively researched for various biomedical applications, included the drugs and genes administration and tissue engineering. The pullulan scaffolds are able to promote the vascular regeneration, the repair of the cardiac tissue and the regeneration of the bone tissue. (37)

1.5. Bone tissue

The bone tissue is part of the specialized connective tissues and it is the principal constituent of the skeleton, the organism support with fundamental structural (providing rigidity, support and

resistance, supporting soft tissues and protecting parts of the body) and metabolic (maintaining a correct homeostatic balance of minerals) functions. (38)

The extracellular matrix represents the 90% of the bone weight, the remaining 10% is constituted by water. The organic matrix in bone tissue is mainly composed of fibrillar type I collagen (≥ 90%) and non-collagenous proteins (10%), such as osteonectin, osteocalcin, and bone sialoprotein. (39) (40)

The structure of bones is divided in levels (macrostructure, microstructure, sub-microstructure, nanostructure, sub-nanostructure) and depending on the level there are variations in the mechanical properties. (41) (42)

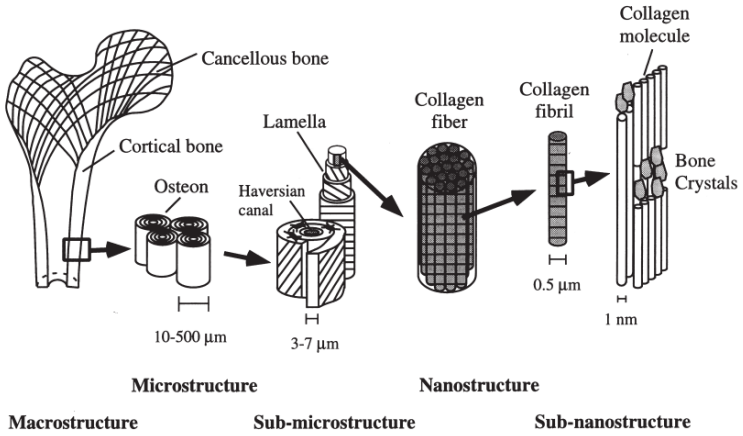

Figure 8 Hierarchical structural organization of bone: cortical and cancellous bone; osteons with Haversian systems; lamellae; collagen fiber assemblies of collagen fibrils; bone mineral crystals, collagen molecules, and non-collagenous proteins. (41)

1.5.1 Hydroxyapatite

Hydroxyapatite (HAp) is a biocompatible ceramic produced through a high-temperature reaction and is highly crystalline form of calcium phosphate. The mineral phase of the bone that forms the vertebrate skeleton is a basic calcium phosphate that is assimilated to HAp. (43) The most important property of this material is, in fact, its chemical similarity to the mineralized phase of bone and this similarity explains the osteoconductive potential and excellent biocompatibility. (44) HAp remains the most intensely studied bioceramic for its biocompatibility as a scaffold material in tissue engineering. (45)

There are several forms of calcium phosphate that make up the apatite family. They are one of the most complex families of materials due to the myriad of phosphate compounds. In addition, the stability of each of the phosphates is influenced not only by small variations in composition, but also by variations in pH and reaction conditions such as solvent, temperature, pressure, nature of precursors and complexing agents used to control the kinetics of the phosphate reaction. It is this complexity that makes these materials very unique and one of the most interesting class of inorganic biomaterial. (45)

1.5.2. Structure and properties of hydroxyapatite

The general chemical formula for apatites is M_{10} (XO_4) $6Z_2$, where M represents a bivalent cation, XO_4 represents a trivalent anion and Z represents a monovalent anion. Depending on

the different ionic substitutions, it is possible to obtain apatites of varying nature, different in composition and properties. (46) The most common form of apatite is hydroxyapatite (HAp) and the nominal composition of this mixture is $Ca_{10}(PO4)_6(OH)_2$ with a calcium-to-phosphate atomic ratio of 1.67. (44) (47) (48) HAp has a hexagonal structure (where axes a and b coincide) with $P6_3/m$ type spatial groups, or with symmetry axis, a triple helix and a specular plane, and is characterized by the following cellular parameters: Axis a = Axis b = 9,418 Å; Axis c = 6,880 Å.

Figure 9 shows the arrangement of atoms in the hydroxyapatite unit cell at projection [001]. Hydroxyapatite has a structure composed of $PO4^{-3}$ ion tetrahedra, in which two oxygen atoms are in the horizontal plane, while the other two are positioned on the axes parallel to the c axis. The arrangement of the tetrahedron is such that two independent cationic sites of crystallography are created. Site I Ca atoms are aligned in columns parallel to the c axis, while Site II Ca atoms are placed at the vertices of the equilateral triangles, which delimit the channels parallel to the c axis and represent the preferred access pathway for the incorporation of foreign ions. (49)

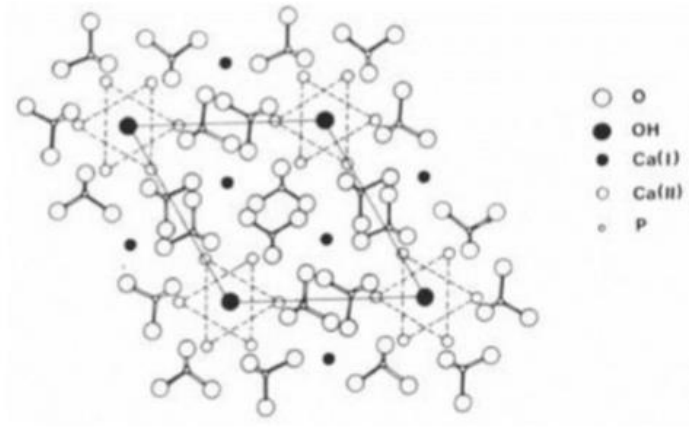

Figure 9 Projection of the constituting ions of HAp on the basal (001) plane

HAp is characterized by a very high resistance to degradation, which is why its resorption occurs over several years. It is free from any form of immune reaction, transmission of disease and pathology at the implant site and is therefore considered a safe and convenient alternative to other alloplastic, heterologous and autologous grafts. (50) (51) (52) Regarding the physicochemical properties of this material, it is characterized by high melting temperature, hardness, high compressive strength. The table shows the main mechanical properties of synthetic hydroxyapatite, which differ in part from biological because they depend on the process with which the crystals were formed. (52)

Table 1 Mechanical properties of hydroxyapatite (52)

Properties	HAp
Young Modulus (GPa)	40-117
Compressive strength (MPa)	294
Tensile strength (MPa)	147
Density (g/cm^3)	3,16

This ceramic is also characterized by a good biocompatibility due to the fact that it is one of the natural constituents of human bones, and bioactivity: in fact, it is able to form bonds with bone tissue, stimulating its regeneration. (45) As for bio absorption, it is favored by the presence of porosity. Porous hydroxyapatite has mechanical characteristics inferior to compact hydroxyapatite but very similar to those of cancellous bones. (53) The presence of 250-500 µm pores creates the ideal microenvironment for bone regeneration and also accelerates the dissolution process thanks to the larger specific surface area compared to a dense ceramic material. (54)

In addition, nanometer sized HAp may have other special properties due to its small size and large specific surface, a significant increase in protein adsorption and osteoblast adhesion in nanometer ceramic materials has been demonstrated compared to traditional ceramic micrometer sized materials. (55)

1.5.3. Hydroxyapatite solubility

Many studies have treated the solubility of hydroxyapatite in aqueous solutions and a large number of solubility constants have been reported, ranging from 10^{-49} and 10^{-59}. Several mechanisms have been proposed to clarify the dissolution behavior of hydroxyapatite: Variations in solubility can be attributed to differences in the rate of formation and dissolution of an intermediate solid phase on the surface, such as $CaHPO_4 * 2H_2O$ (brushite) and $CaHPO_4$ (monetite). (56) Solubility of hydroxyapatite increases with decreasing pH.. Surface ions are kept below internal ions and therefore can be more easily dissolved. Crystalline defects, such as impurities may affect the dissolution phenomenon. The chemical reactivity of solids varies inversely with their crystalline perfection and crystal size. (57) (58)

1.5.4. Biological and synthetic hydroxyapatite

Hydroxyapatite and calcium phosphate ceramic materials have been widely used as implant materials because of their close resemblance to the natural bone composition. Chemically and structurally, HAp with the stoichiometric formula $Ca_{10} (PO_4)_6 (OH_2)$ and a molar ratio Ca / P = 1.67 is the material most similar to the inorganic part of bones and teeth. Both dense and porous HAp have been studied as implant materials for orthopedic and dental applications, presenting excellent bioactivity, osteoconductivity and osteoinductivity. However, there are differences in comparing synthetic and natural hydroxyapatite in terms of crystallography and composition. (59)

A lot of differences in composition and crystallography can be found between the biological and the synthetic hydroxyapatite. The biological HAp is entirely constituted from Ca, PO_4^{3-} and OH^- ions, while the synthetic HAp contains even other ions that enter the crystalline structure after ionic substitutions or adsorption on the surface and that may alter some of its structural and chemical-physical properties, such as morphology, crystallinity, thermal stability and solubilization, but with no changes in the crystalline structure.

Also magnesium, due to its relatively high presence in mineralized tissues, plays a key role in the activity of biological apatite. In particular, the presence of Mg^{2+} ions in substitution for Ca^{2+} ions accelerate HAp nucleation kinetics, but inhibits crystallization in solution, causing

reduction in Ca / P molar ratio and crystallite size. The incorporation of Mg^{2+} ions can alter the morphology and solubility of the biomineral and, as a major inhibitor of apatite crystal growth, influences its size and reactivity. (60)

1.5.5. Biomedical use

Ceramics are mainly used as bone substitutes in the biomedical industry due to their biocompatibility, low density, chemical stability, high wear resistance and with respect to calcium phosphates, mainly due to their compositional similarity to the bone mineral phase. However, the potential of any ceramic material to be used as a plant in vivo depends on its ability to withstand complex stresses at the application site and its compatibility with the biological environment. (61)

In particular, HAp has been widely used for biomedical implants and bone regeneration applications and to overcome some of its limitations, it has been used in combination with polymers or other materials to form compounds. Thanks to its similarity to inorganic components of bone structure, synthetic hydroxyapatite was one of the first materials used. (62)

2 Objective

Tissue engineering aims to regenerate damaged tissues instead of replacing them, by developing biological substitutes, which are polymeric scaffolds able to simulate the characteristics of the extracellular matrix and to act as a support for tissue growth encouraging the adhesion, migration, proliferation and differentiation of the cells. Electrospun nanofibrous membranes have been developed, which have a homogeneous morphology that makes them ideal substrates for cell growth and tissue regeneration.

The objective of the thesis was the development of scaffolds formed by the polymeric material in order to create supports for the regeneration of tissues. It consisted in the preparation and characterization of the polymeric solutions. The solutions were prepared with biocompatible and biodegradable polymers: chitosan was associated with pullulan, a polymer widely studied in literature for its electrospinning capability. The solutions were created with different concentrations (0,1% and 0,5%) of hydroxyapatite, which is a calcium phosphate chemically similar to the bone mineral phase. The solutions were characterized in terms of consistency, superficial tension and conductivity. The polymeric solutions were then electrospun with electrospinning technique at high voltages both on a static collector, that allows to obtain nanofibers randomly oriented, and on a rotating collector, that allows to obtain nanofibers with an aligned orientation. The wettability was also studied for the scaffold randomly and aligned oriented. The electrospun nanofibers were morphologically analyzed with a Scanning Electron Microscope (SEM). The mechanical properties of the scaffolds in random configuration and in aligned configuration were also evaluated, in dry and hydrated state with a Texture analyzer.

3 Materials

Polymers:

- Chitosan, deacetylation degree 98%, MW 251000 Da, maximum charge density: number of functional groups positively charged for repetitive unit: 0,98 (ChitoClear, Siiiglufjordur-Iceland);
- Pullulan, Food grade (Hayashibara, Okayama-Japan);
- PVP K-120 (ISP Europe-England).

Powders:

- Citric acid (Carlo Erba Reagents, Italy);
- Hydroxyapatite, nanopowder < 200 nm particle size, ≥ 97% synthetic (SigmaAldrich, USA).
- Maltodextrin, dextrose equivalent 16.5-19.5 (Sigma-Aldrich, USA).

Solvents:

- Acetic acid (Carlo Erba Reagents, Italy).

4 Methods

4.1 Preparation of polymeric solutions

First was prepared a polymeric solution based on pullulan and chitosan. This solution was obtained by mixing two other polymeric solutions in a 1:1 ratio. This mixture was made using magnetic agitation at room temperature. The first solution was prepared by solubilizing the 20% of pullulan (PLL), in milliQ water, either alone or in a mixture whit hydroxyapatite (HAp). The second solution was prepared by solubilizing the 5% of Chitosan (CH) in Acetic acid 90% and then the 5% citric acid was added as well.

We chose to use two different HAp concentrations, the 0,1% and the 0,5%, so that we get nanofibers containing a concentration of hydroxyapatite that could improve their mechanical properties (Table2). This solution was obtained by mixing two other polymeric solutions in a 1:1 ratio and also was made using magnetic agitation at room temperature.

A solution based on PVP (Polyvinylpyrrolidone) was also prepared to obtain nanofibers with greater mechanical properties. The first solution was prepared by solubilizing the 30% of PVP in milliQ water. The second solution was prepared by solubilizing the 60% of Maltodextrin (MDX) in distilled water. 2% HAp was added to obtain nanofibers with better mechanical properties. (Table 3.)

Table 2 Qualitative and quantitative composition of the solutions

Polymeric solution	Pullulan % (w/w)	Chitosan % (w/w)	Citric Acid % (w/w)	HAp % (w/w)	Acetic Acid % (w/w)
F1	10	2.5	2.5		45
F2	10	2.5	2.5	0.1	45
F3	10	2.5	2.5	0.5	45

Table 3 Qualitative and quantitative composition of the solutions

Polymeric Solution	PVP % (w/w)	Maltodextrin % (w/w)	HAp % (w/w)
F4	15	30	
F5	15	30	2

4.2 Characterization of the polymeric solutions

4.2.1 Measurement of consistency

The measurement of consistency was made using the Texture Analyzer TA.XT plus (ENCO, Spinea, I), equipped with a cylindrical Perspex probe with the diameter of 20 mm (P/20P, batch No. 11434) and the samples were placed in a thermostatically-controlled water bath at 30°C, which is the electrospinning temperature of the solutions. The parameters for the experiment were: pre-test speed: 1 mm/sec; test speed: 0,50 mm/sec; post-test speed: 10 mm/sec; trigger mode: Distance; trigger Force: 0,10 mN; distance: 3 mm.

To evaluate the solution consistency, it was evaluated the sinking force of the probe in the polymeric solution, that is influenced by the material characteristics, the temperature and the force applied on the probe.

4.2.2 Surface tension

For the surface tension, was used an automatic tensiometer (DY-300 Kyowa), equipped with a platinum plate of 2,5cm x 1cm. Before starting the analysis, the solutions were heated at 30°C for 15 minutes, the same temperature of the electrospinning process. The instrument registered a tension value every 3 seconds for a total time of 300 seconds. For each solution were run three repetitions, with different immersion distances of the plate of 0,2 mm, 0,5 mm and 1 mm.

4.2.3 Conductivity

The conductivity was evaluated using a portable conductivity meter FiveGo F3 - Mettler Toledo. It was calibrated before starting the analysis using two solutions with a known conductivity of 1413 µS/cm and 1288 µS/cm.

4.2.4 X-ray diffraction

X-ray diffraction allows to study the structural characteristics of crystalline and amorphous matter, and the determination of the type of atoms present, their distribution and the distances between the atomic planes, these properties allow identification.

The polymeric solutions were analysed with a diffractometer (Buker D8 Advance) with a copper cathode source. The instrument works on the basis of the Bragg's law.

This analysis was performed on the polymeric solutions and on the acid solutions without polymer. The solutions under examination were put on a glass support and dried for 10 minutes with a hot source, then they were taken to the instrument for the analysis.The hydroxyapatite is in a very low quantity, so the x-rays, which interact with the electron clouds of atoms, have to stay with the samples for a longer time to get a better signal. The scan range goes from 20° to 60°; The X-rays invest the sample, the instrument counts 20 seconds and then the arms move of 0,02°. The instrument is connected to the program Diffrac plus XRD commander, that registers the signal after the interaction with the sample.

4.3 Electrospinning (polymeric solutions)

The solutions (Table 2 and 3) were electrospun with an electrospinning (STKIT-40, Linari Engineering). The electrospinning is composed of a collector, which can be an aluminium foil on a support or a rotating collector, a volumetric pump (Razel R99-E), a glass syringe of 10 cc with an inox needle, and an high voltage generator (5-40 kV). (Fig.10)

The electrospinning process was done at atmospheric pressure, with the temperature between 25-35°C and the relative humidity (RH) between 25-35%.

The electrospinning parameters (voltage, flow rate, distance between the tip of the needle and the collector, needle diameter) were adapted to the characteristics of the solutions in order to obtain a continuous and uniform flow that allows the formation of fibres without imperfections.

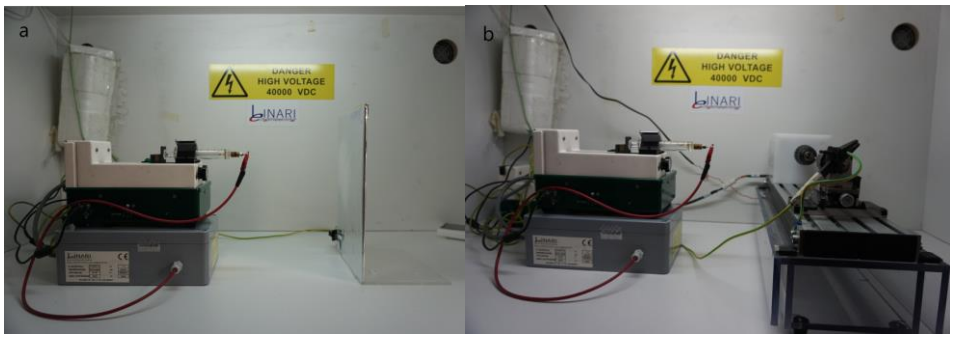

Figure 10 Electrospinning STKIT-40 Linari Engineering with a static collector (a) and a rotating collector (b)

Parameters used for the solutions of the Table 2 and 3:

Table 4 Electrospinning parameters of the solutions in Table 2 and 3

Solution	Distance (cm)	Voltage (kV)	Flow (cc/hr)	Needle diameter (m/m)
F1	15	22	0.397	0.8
F2	15	20	0.397	0.7
F3	15	20	0.397	0.7
F4	14	28	0.397	0.8
F5	14	28	0.397	0.8

Was used two different types of collectors, for the electrospinning of the polymeric solutions, to obtain fibres with a different orientation.

Basically, a static collector and a rotating collector were used. One was the static collector (Fig.10a), that is composed of an aluminium foil placed on a vertical plate of acrylic/pexiglass for support (on a plexiglass support), on which the fibres were randomly oriented using the spinning parameters in Table 4. The other is the rotating collector (Fig.10b), that is composed of a rotating cylinder of inox steel which can be of different diameters and allows to obtain fibres with an aligned orientation, differently of the randomly orientation of the static collector. This aligned orientation is possible due to two different movements of the collector: a clockwise motion of the collector around the axis and a longitudinal movement along the axis. The rotation of the collector around the axis is regulated by a rotation speed control unit and by a rotation unit that mechanically allows the effective rotation of the collector and its substitution. On the control unit the frequency value is reported in Hertz (Hz) and the rotation speed is regulated by this equation: V = F*15 rpm (revolutions per minute). The frequency range goes from 5 Hz to 200 Hz, while the rotation speed range goes from 75 rpm to 3000 rpm; the frequency used in this case was 200 Hz (3000 rpm). The longitudinal movement of the collector along the axis is controlled by a plexiglass support (speed of 60 oscillations per minute).

The F4 and F5 solutions were electrospun as inner layer of the tubular scaffolds with F1, F2 and F3 solutions to improve their mechanical properties (Fig.11). The collector diameters used were 0,8 mm and 3 mm.

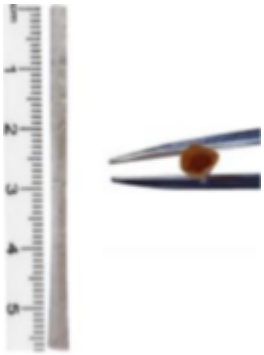

Figure 11 Nanofibers electrospun in tubular conformation with a rotating collector of inox steel

4.3.1 Nanofibers cross linking process

Right after the electrospinning process, the nanofibers were cross-linked to make them insoluble in an aqueous medium. For the cross-linking process, the fibres were put in a heater at 150° for about 60 minutes.

4.4 Characterization of the nanofibers

4.4.1 Solubility test

To test the solubility of the nanofibers we immersed them in milliQ water for 1 hour. All of the nanofibers obtained from the polymeric solutions described in Table 1 were resistant to the solubility test.

4.4.2 Scanning Electron Microscope (SEM)

The Scanning Electron Microscope is a type of microscope that produces images of a sample by scanning its surface with a focused beam of electrons. With the SEM analysis it is possible to obtain morphological images of the surface topography and black-and-white images based on the atomic number (Z) of elements, that informs about the sample composition.

The analysis was performed at the CISRiC (Centro Interdipartimentale di Studi e Ricerche per la Conservazione dei beni culturali) by the doctor Ilenia Tredici with a scanning electron microscope Tescan, Mira3.

To make the samples conductors, they were spattered with platinum through a vapor deposition under vacuum and the images were captured with a high vacuum process at a voltage of 8.0 kV at room temperature. Different enlargements were captured: 10.0 kx (5µm), 5.00 kx (10 µm) and 2.00 kx (20 µm). The configuration of F1, F2 and F3 fibres as electrospun were observed, both random and aligned, and also the configuration of F2 and F3 fibres after 6 days of hydration were observed to assure the maintenance of the aligned orientation of the tubular scaffolds.

4.4.3 Transmission Electron Microscope (TEM)

The transmission electron microscope (TEM) is used for studying low-dimensional materials, such as hydroxyapatite. The intrinsic capability of TEM for imaging also allows to map the isotope concentration in selected nanoscale areas, such as the polymeric fibres.

A thin layer of fibre was electrospun directly onto the TEM grids and put in a heater at 150°C for 2 minutes, inducing the cross-linking process. The analysis was conducted at the CGS (Centro Grandi Strumenti, Università di Pavia) by the doctor Massimo Boiocchi.

TEM observations were carried out on a JEOL JEM-1200 EX II microscope operating at 100 kV (tungsten filament gun) and equipped with the TEM CCD camera Olympus Mega View G2 with 1376 X 1032-pixel format. The photos of the samples were taken with the following magnifications: 15k, 50k.

4.4.4 Contact angle

The contact angle and it is one of the principal parameters to evaluate the wettability of a surface. As shown in figure 12, it is the angle formed between the liquid and the solid surfaces, quantifying its level of wetting. (63)

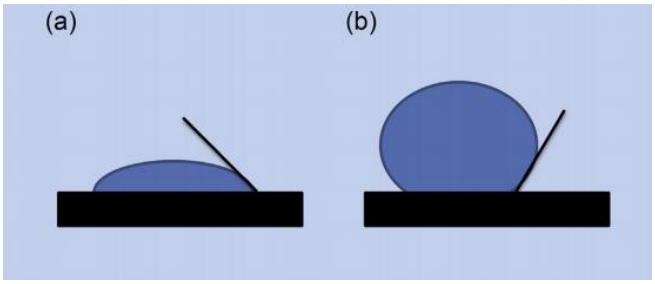

Figure 12 Contact angle of a water drop with a solid surface; <90° indicates wetting (a) and ≥90° indicates nonwetting (b). (63)

The wettability of the electrospun fibres was evaluated with a Contact Angle Meter DMe211 Plus connected to a FAMAS software.

The measurements were conducted in the time-based mode, capturing a droplet of 0,4 µl continuously to study the interfacial tension variations over time. The droplet was captured every 100 msec for 10 times with an ending time of 1000 msec. The cross-sectional view of the droplet shape was captured through the CCD camera of the instrument.

4.4.5 FT-IR Spectroscopy

Infrared spectra of the fibres, were recorded with Fourier transform infrared spectrometer (FT-IR, Spectrum BX, Perkin Elmer). As a proof of the presence of hydroxyapatite before and after the cross-linking process we used the FT-IR so we could detect chemical compounds into the fibres. It is equipped with an optical system covering the range 7800-350 cm-1 with a resolution of < 1 cm-1. The calibration was performed before starting the analysis, scanning the background in single-beam mode. All samples were put in the sample compartment and measured in transmission mode, in the frequency range of 4000-400 cm-1 and the resolution of 1 cm-1;

The FT-IR spectroscopy results of the fibres with hydroxyapatite were compared to the results of the blank fibres to evaluate the effective presence of the mineral. The results of the cross-linked fibres with HAp were compared to the results of the not crosslinked fibres make sure that there were no changes caused by the cross-linking process.

4.4.6 Analysis of the mechanical properties

For the analysis of the mechanical properties of the nanofibers, the TA.XT plus texture analyzer (ENCO, Spinea, I) was used. This instrument is equipped with an A / TG measuring system consisting of two clamps with serrated faces 35x35 mm in size, fixed to the equipment by special screws.; the lower clamp is fixed while the upper is movable, to allow the sample analysis.

The evaluation of the mechanical properties was executed on the fibres with random orientation and on the fibres with aligned orientation. In the last case, the properties were evaluated in a closed tubular configuration. In all the cases was necessary to cut the fibres, the dimensions of the pieces are described in Table 5.

Table 5 Dimensions of the fibre pieces for the analysis of the mechanical properties

	Dimensions	**Thickness**
Random fibres	3cm x 1cm	0,2-0,3 mm
Closed tubular	2cm x 0,5 cm	0,4-0,5 mm

The thickness of the fibres was measured with a quadrant feeler gauge Sicutool 3955G-50, putting the membrane on the support and reading its thickness through the two quadrants.

All the analysis was performed with the 5 kg load cell. Each sample was inserted between the clamps so that the exposed surface was 1 cm x 1 cm for the random fibres, 1 cm x 0,5 cm for the closed tubular, 1 cm x 1 cm for the long side of the open tubular and 0,5 cm x 0,5 cm for the short side of the open tubular.

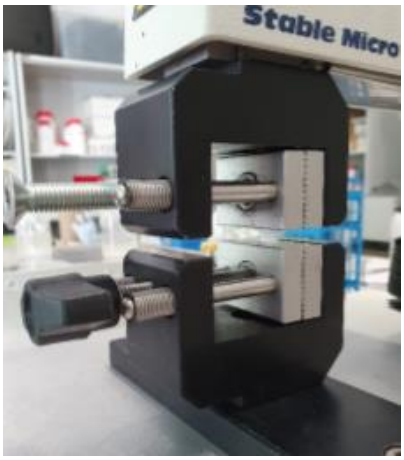

Figure 13 TA.XT plus Texture Analyser (ENCO, Spinea I) equipped with two clamps for the fibres mechanical properties analysis

The instrument is connected to a computer and through a program (Exponent) it is possible to start the analysis. The instrument was first calibrated, then the parameters set up were: project speed (1 mm/sec), test speed (0,5 mm/sec), post-test speed (5 mm/sec), trigger mode (Distance), trigger Force (0 mN), distance (30 mm).

The analysis were performed in dry state,and wet state (hydrating the fibres with sprayed water). When the analysis starts, the upper clamp move up, causing the tensile of the fibre until it is broken. The applied force increases as the distance covered by the clam increases, up to a

maximum that corresponds to the complete rupture of the fibre used. Beyond this point of maximum force there is a decrease of this parameter in function of the movement.

The values of the maximum force (breaking force) were analysed, normalizing this force value to the fibre area placed between the clamps, and the values corresponding to the elongation % were calculated by dividing the distance covered by the clamps for the initial distance. With these results it was possible to construct a graph to evaluate the maximum force compared to the elongation (%) of the fibres.

5 Results and discussion

5.1 Characterization of the polymeric solutions

5.1.1 Consistency

Figure 14 reports the penetration profiles as force (mN) vs distance (mm) evaluated for F1, F2 and F3. The consistency of F1 without Hap in suspension is significantly higher than those of F2 and F3 which present similar profiles regardless of Hap concentration. The presence of Hap in suspension decreases the consistency of polymeric blends probably due to an interaction between Hap and polymers that could change polymer three-dimensional network.

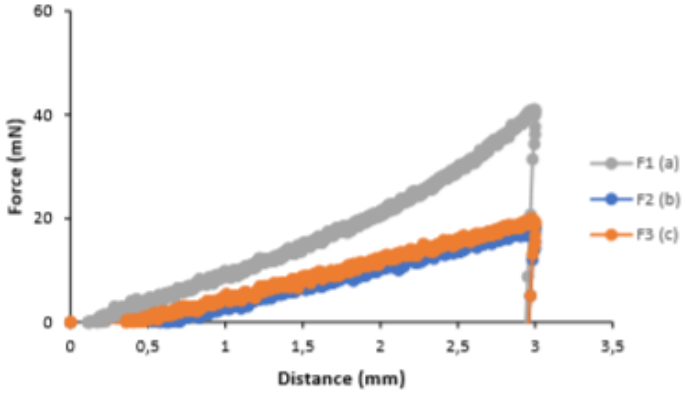

Figure 14 Penetration profiles evaluated for F1 (polymeric blend based on PLL and CH), F2 and F3 (polymeric blend having the same composition as F1, but containing hydroxyapatite HAp at 0,1% or 0,5% w/w)

5.1.2 Surface tension

Figure 15 shows the values of surface tension (mN/m), evaluated for F1, F2 and F3. The surface tension seems to be inversely proportional to the consistency of the solution: F1 shows a higher consistency and a lower surface tension, on the other hand, F2 shows a lower consistency and a higher surface tension. F3 shows a surface tension lower than that of F2 but higher than that of F1.

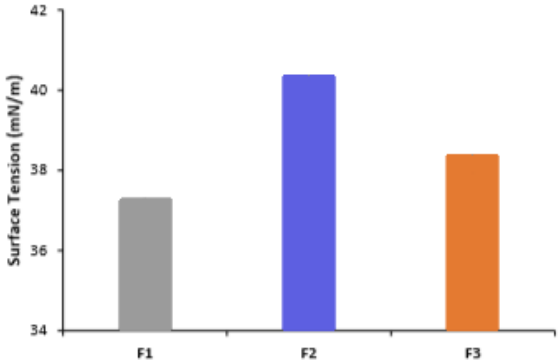

Figure 15 Values of surface tension (mN/m) evaluated for F1 (polymeric blend based on PLL and CH), F2 and F3 (polymeric blend having the same composition as F1, but containing hydroxyapatite HAp at 0,1% or 0,5% w/w)

5.1.3 Conductivity

Figure 16 reports the conductivity values (µS/cm) for F1, F2 and F3. The presence of Hap increases the conductivity and this seems to be directly related to the increase of HAp concentration. F1 has the lower conductivity.

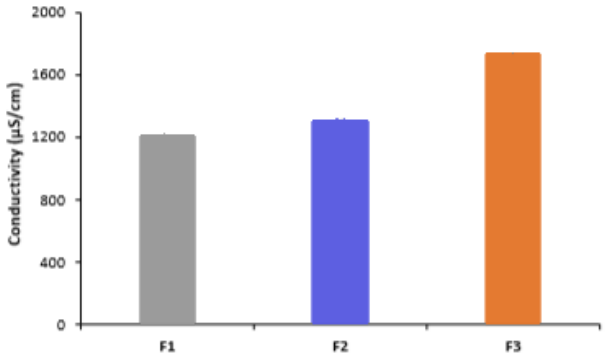

Figure 16 Values of conductivity (µS/cm) evaluated for F1 (polymeric blend based on PLL and CH), F2 and F3 (polymeric blend having the same composition as F1, but containing hydroxyapatite HAp at 0,1% or 0,5% w/w)

5.1.4 X-ray diffraction

Figure 17 reports the diffraction profiles of the HAp as powder (particle size 200 nm) and of the Hap suspended in water and in acetic acid at 0,1% w/w concentration.

HAp at 0,1% w/w concentration seems to maintain its crystallinity independently of the solvent in which it is dispersed.The X-ray diffraction spectra of HAp, as suspensions both in water and in acid, show characteristic peaks of the hydroxyapatite powder.

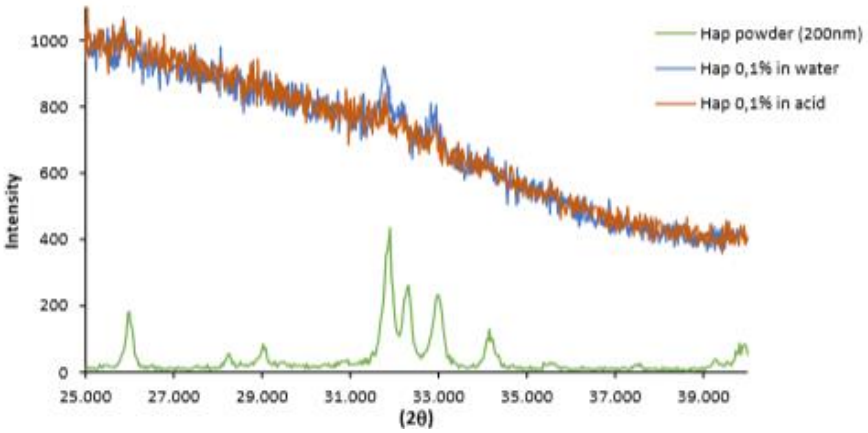

Figure 17 X-ray diffraction of the HAp powder (200 nm) compared with the HAp 0,1% in water and with the HAp 0,1% in acetic acid

5.1.5 Scanning Electron Microscope (SEM)

Figure 18 shows the SEM images of the F2 formulation (HAp 0,1%) without polymer compared with a solution of water with the 0,1% of HAp. Figure 9 shows that the lower concentration of HAp (0,1%) is characterized by spherical particles present both in water and acid solution. The Hap particle size is extremely different dependently of the medium used: when in water the Hap powder presents a fine fraction and few particles having bigger dimensions. In acid solution,

Hap particles have greater dimensions and this is probably due to the solubilization of the fine fraction.

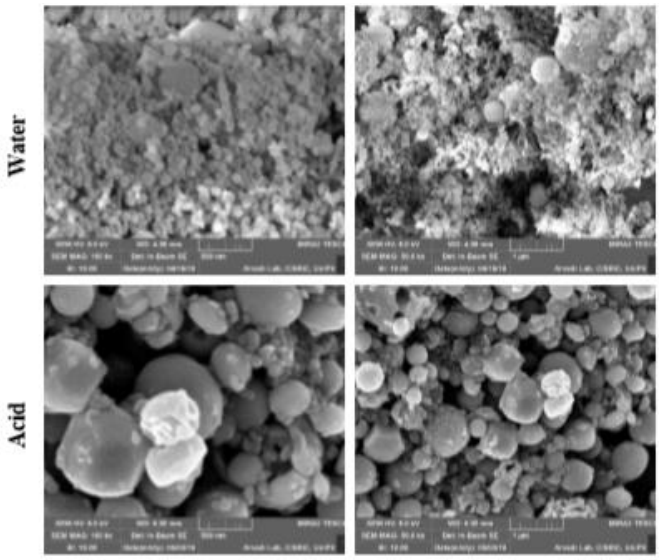

Figure 18 SEM images of the F2 formulation (HAp 0,1%) without polymer compared with a solution of water with the 0,1% of HAp at two different magnifications (100 kx and 50.0 kx)

5.2 Morphological characterization

5.2.1 Scanning Electron Microscope (SEM)

Figure 19 shows the SEM images of the F1, F2 and F3 formulations randomly collected.

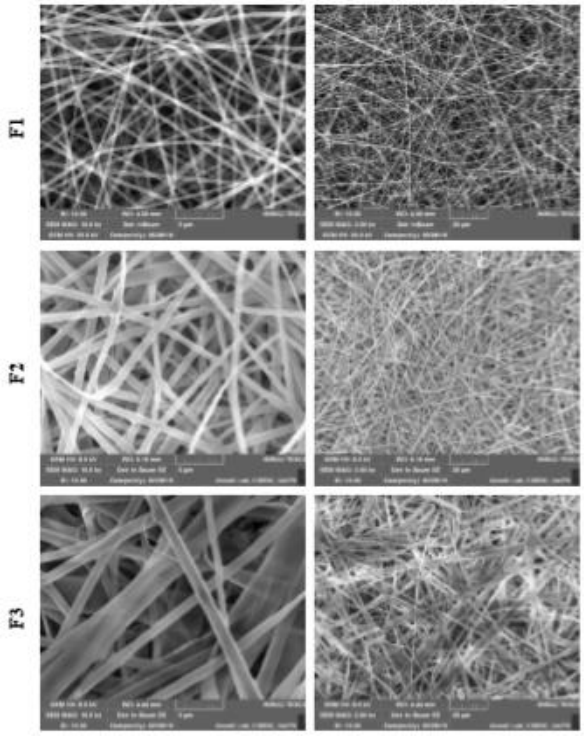

Figure 19 SEM images of the F1, F2 and F3 formulations randomly collected at two different magnifications (10.0 kx and 2.00 kx)

Figure 20 shows the SEM images of the aligned F1, F2 and F3 nanofiber-based scaffolds, reinforced with F4 and F5 as inner layer.

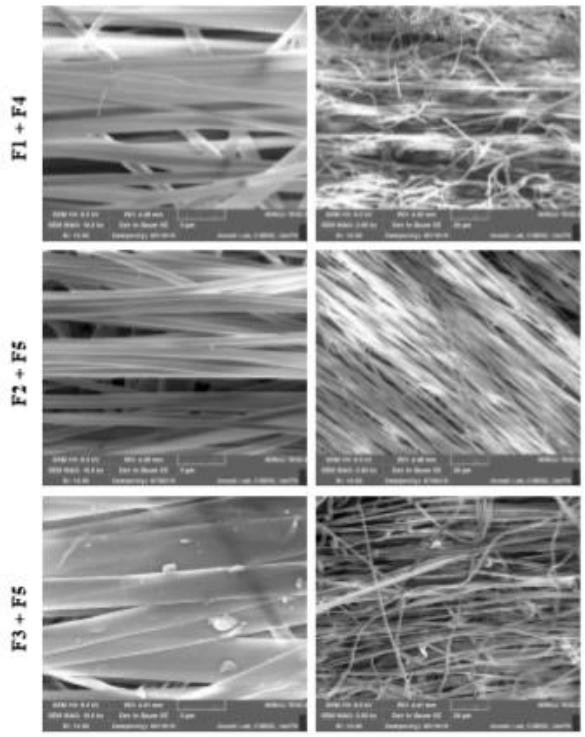

Figure 20 SEM images of the aligned F1, F2 and F3 nanofiber-based scaffolds reinforced with F4 and F5 at two different magnifications (10.0 kx and 2.00 kx), collected with 3 mm drum

F1 scaffold is characterized by nanofibers with regular morphology and smooth surface, while the presence of HAp in F2 and F3 determines nanofibers with a higher roughness and the presence of aggregates (probably due to HAp nanoparticles).

Figure 21 reports the SEM images of the aligned F2 and F3 nanofiber-based scaffolds, reinforced with F5 as inner layer, after 6 days of hydration in water.

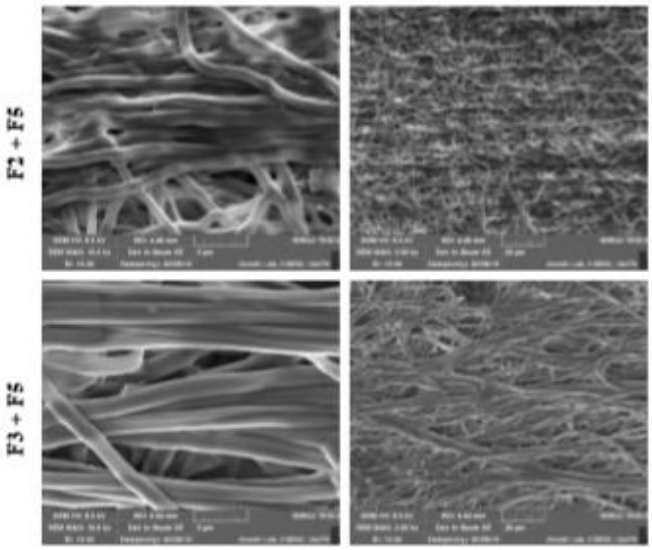

Figure 21 SEM images of the aligned F2 and F3 scaffolds, reinforced with F5 after 6 days of hydration, at two different magnifications (10.0 kx and 2.00 kx)

The fibres obtained from F2 and F3 scaffolds seem to maintain their aligned configuration after 6 days of hydration although a partial swelling happened.

5.2.2 Transmission Electron Microscope (TEM)

Figure 22 shows the TEM images of the F1 and F2 formulations. The F2 images show the inclusion of hydroxyapatite particles into the nanofiber structure.

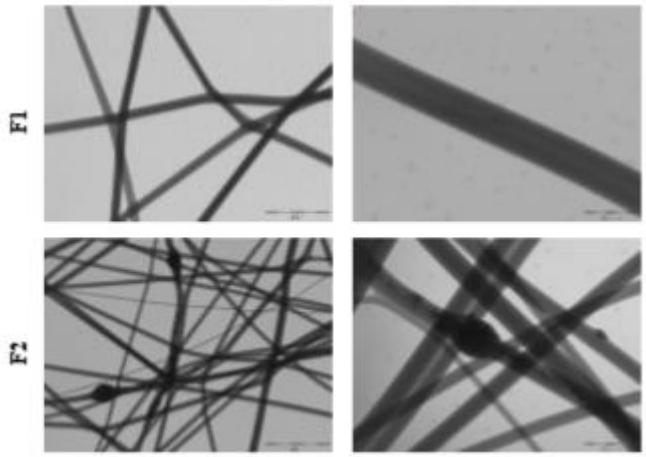

Figure 22 TEM images of the F1 and F2 formulations at two different magnifications (15k and 50k)

5.2.3 Wettability evaluation

Figure 23 shows the values of the contact angle for the F1, F2 and F3 formulations randomly collected. The scaffold without Hap nanoparticles shows a higher contact angle (deg), so it seems to possess a lower wettability. The presence of HAp into the fibres increases their wettability independently of its concentration.

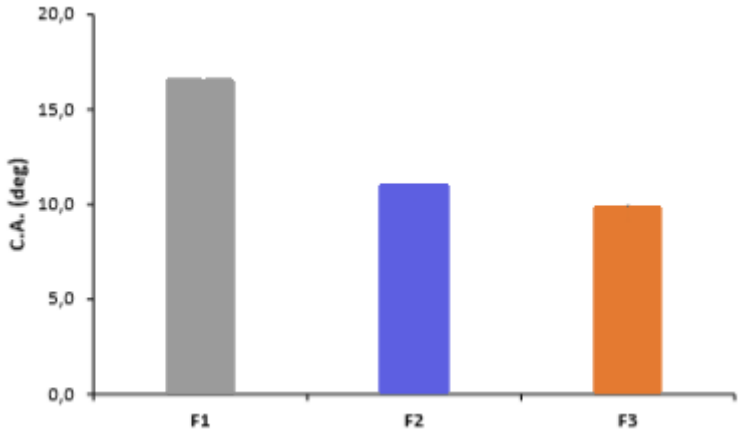

Figure 23 Values of the contact angle (deg) of F1, F2 and F3 scaffolds randomly collected

5.2.4 FT-IR analysis

Figure 24 reports the FT-IR spectra of the hydroxyapatite powder. (64) As reported in literature, the bands at 962 cm−1 and 473 cm−1 are due to the υ1 and υ2 vibrational modes of phosphate group and also the bands at 602 cm−1 and 566 cm−1 represent υ4 vibrational band of phosphate group.The prominent bands at 3417 cm-1 is due to the vibratory stretching of OH group of HAp. (65)

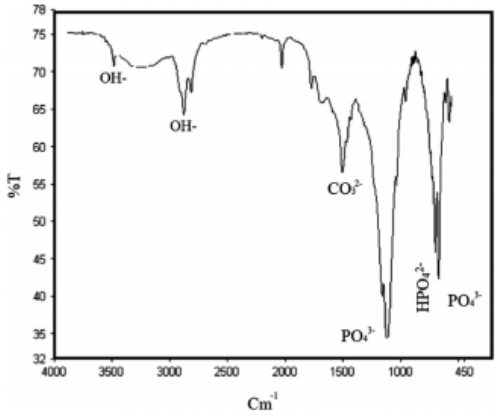

Figure 24 FT-IR spectra of the hydroxyapatite powder (64)

Figure 25 reports the FT-IR spectra of the F1, F2 and F3 scaffolds randomly collected and after cross-linking.

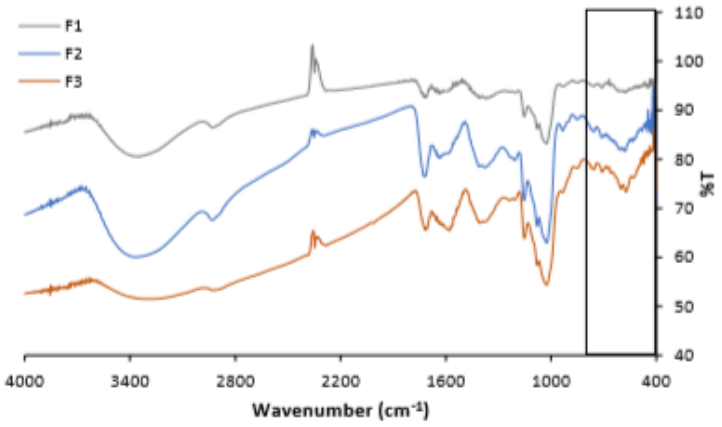

Figure 25 FT-IR profiles of the F1, F2 and F3 scaffolds randomly collected and after crosslinking

No significant differences are shown in the FTIR patterns between blank and HAp-loaded scaffolds; this is probably due to the low content of hydroxyapatite. In the 400-800 cm-1 wavenumber interval, a characteristic band of the phosphate group is shown in the F2 (0,1% HAp) and F3 (0,5% HAp) patterns.

5.2.5 Tensile measures and evaluation of the mechanical properties

5.2.5.1 Tensile measures on fibres randomly oriented

Figure 26 represents the stress-strain curves of the F1, F2 and F3 formulations, both in dry (a) and hydrated (b) state

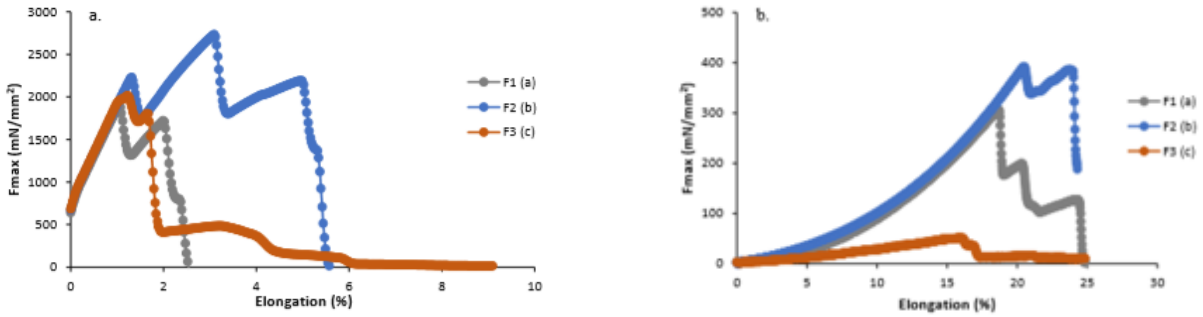

Figure 26 Stress-strain curves evaluated for F1, F2 and F3 formulations both in dry (a) and hydrated (b) state randomly oriented, prepared with a static collector

Figures 27 and 28 represent the maximum tensile force values (mN/mm2) and the values of elongation (%) of the fibres randomly oriented both in dry (a) and hydrated (b) state.

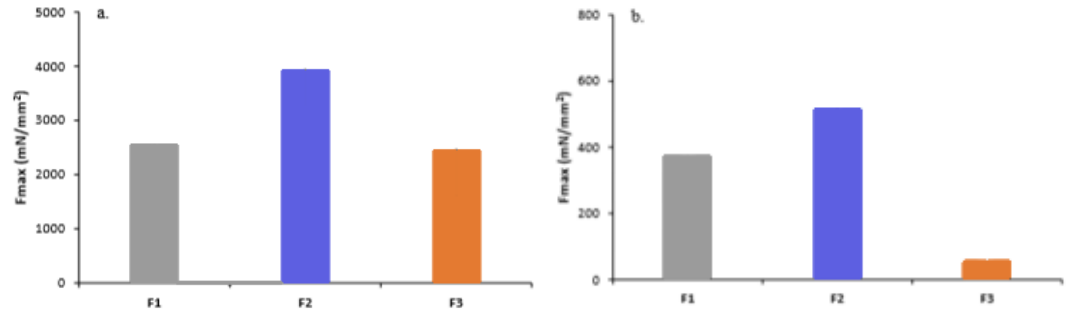

Figure 27 Maximum tensile force values (mN/mm2) evaluated for F1, F2 and F3 formulations both in dry (a) and hydrated (b) state randomly oriented, prepared with a static collector

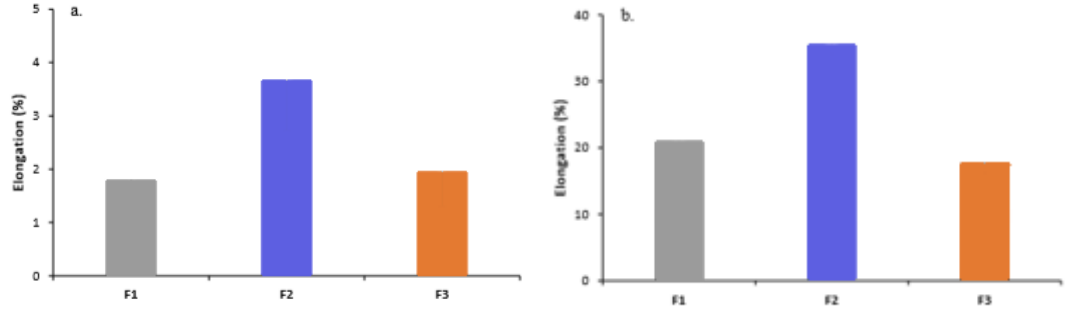

Figure 28 Elongation (%) values evaluated for F1, F2 and F3 formulations both in dry (a) and hydrated (b) state randomly oriented, prepared with a static collector

Figure 29 represents the Young Modulus values (mN/mm2) of the F1, F2 and F3 formulations randomly oriented, both in dry (a) and hydrated (b) state.

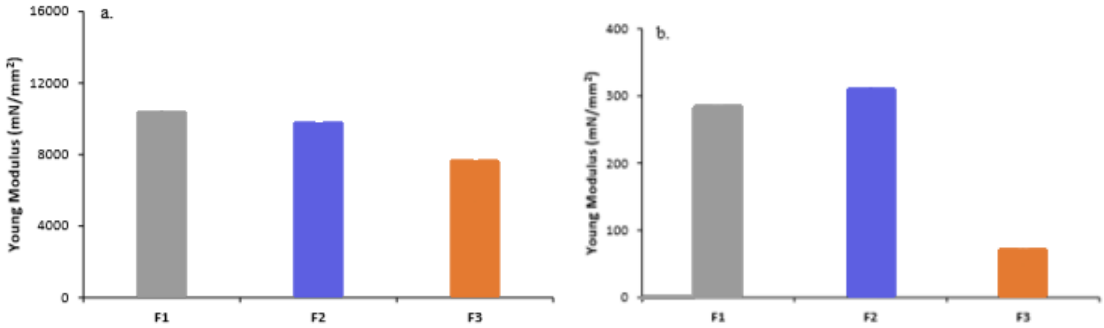

Figure 29 Young Modulus (mN/mm2) values evaluated for F1, F2 and F3 formulations both in dry (a) and hydrated (b) state randomly oriented, prepared with a static collector

5.2.5.2 Tensile measures on closed tubular scaffolds in aligned orientation

Figures 30 and 31 represent the stress-strain curves of the F1, F2 and F3 formulations reinforced with F4 and F5 as inner layer, both in dry (a) and hydrated (b) state, evaluated for the closed aligned scaffolds prepared with two different rotating collectors having the diameters of 0,8mm and 3mm.

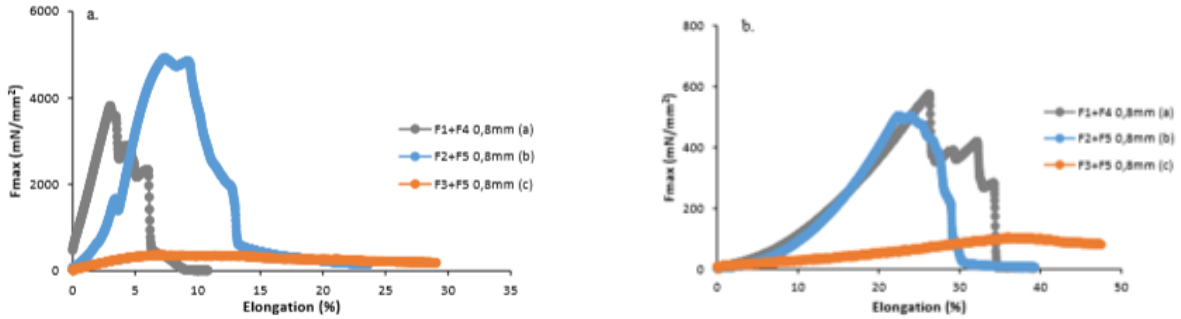

Figure 30 Stress-strain curves of the F1, F2 and F3 formulations reinforced with F4 and F5 as inner layer, both in dry (a) and hydrated (b) state, evaluated for the closed aligned scaffolds prepared with a rotating collector having the diameter of 0,8mm

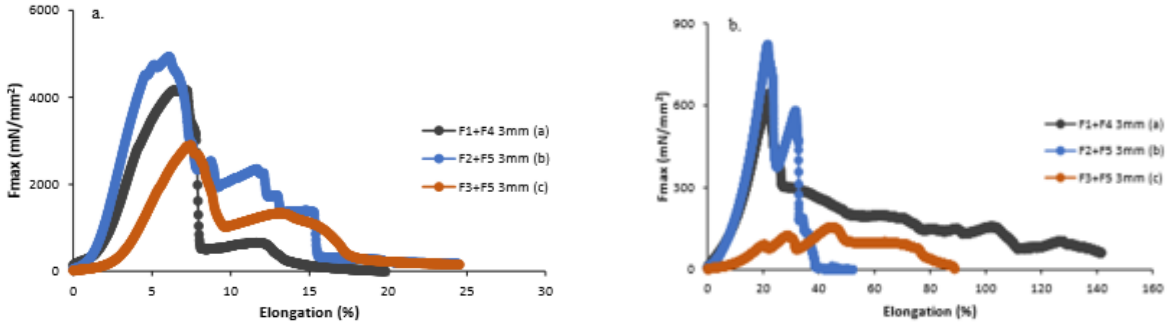

Figure 31 Stress-strain curves of the F1, F2 and F3 formulations reinforced with F4 and F5 as inner layer, both in dry (a) and hydrated (b) state, evaluated for the closed aligned scaffolds prepared with a rotating collector having the diameter of 3mm

Figures 32, 33 and 34 show direct comparison of maximum tensile force, elongation and Young modulus, both in dry (a) and hydrated (b) state, for the scaffolds randomly collected and for the aligned 3D scaffolds, reinforced with F4 and F5 as inner layer. The tubular scaffold with 3 mm diameter seems to have the higher values of maximum tensile force, both in dry and hydrated state, independently of the formulation scaffold type. In the hydrated state, the fibres are more fragile than they are in the dry state, while in the dry state they seem to be poorly deformable, compared to the hydrated state.

The F3 tubular scaffold with 0,8 mm diameter seems to have a significantly higher elongation % in the hydrated state, but a significantly lower maximum tensile force; so, it seems to have a high deformability but a low resistance. The F2 fibres seem to have a higher resistance and deformation, with a maximum tensile force of about 8000 mN/mm2 and a Young modulus of about 20000 mN/mm2 at the dry state and 500 mN/mm2 at the hydrated state. The Young modulus of the F2 tubular scaffold with 3 mm diameter is significantly higher in the dry state while in hydrated state it is comparable with the other scaffolds.

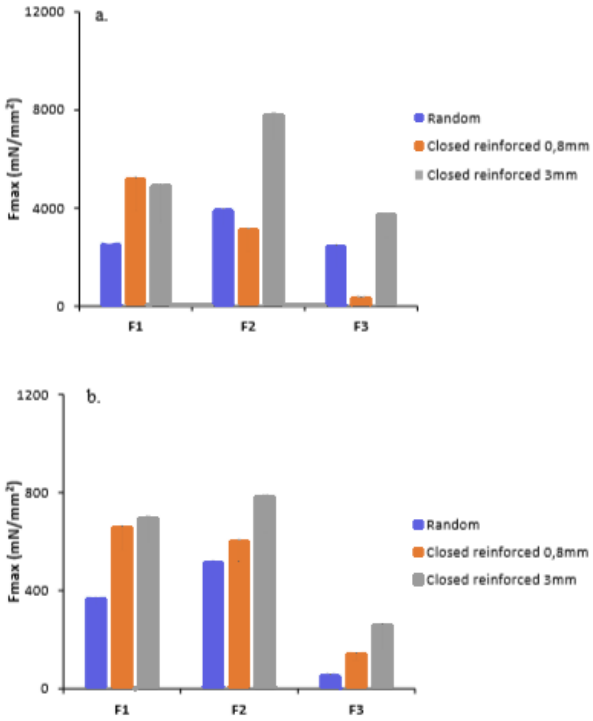

Figure 32 Direct comparison of maximum tensile force (mN/mm2), both in dry (a) and hydrated (b) state, for the scaffolds randomly collected and for the aligned 3D scaffolds, reinforced with F4 and F5 as inner layer

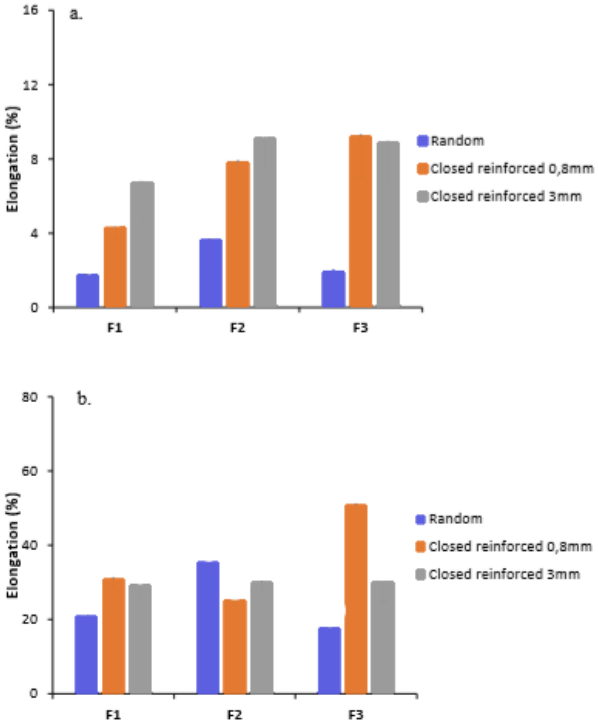

Figure 33 Direct comparison of elongation (%), both in dry (a) and hydrated (b) state, for the scaffolds randomly collected and for the aligned 3D scaffolds, reinforced with F4 and F5 as inner layer

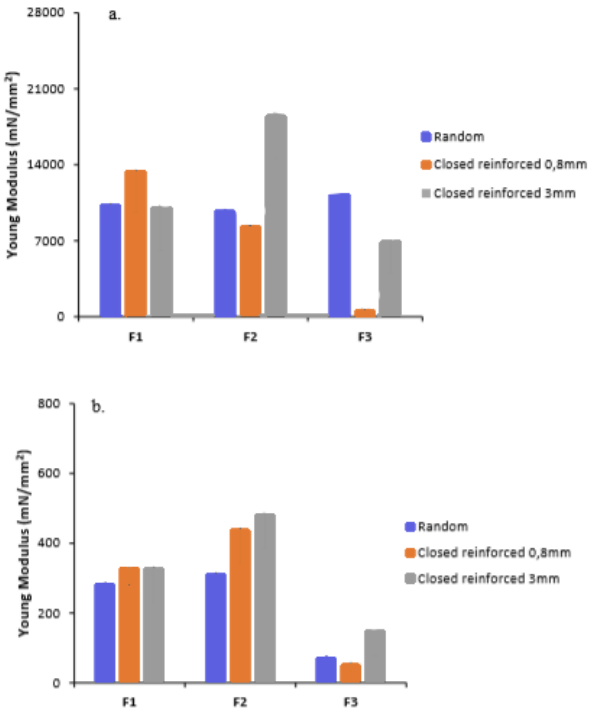

Figure 34 Direct comparison of Young modulus (mN/mm2), both in dry (a) and hydrated (b) state, for the scaffolds randomly collected and for the aligned 3D scaffolds, reinforced with F4 and F5 as inner layer

6 Conclusion and future perspectives

With this study I can conclude that it was possible to prepare nanofibrous 3D scaffolds containing hydroxyapatite. The composition considered was based on pullulan, chitosan, citric acid and acetic acid. Two different concentrations of hydroxyapatite were used, by mixing into the polymer blends to obtain HAp-loaded scaffolds. Polymer blends were physically characterized by consistency, surface tension and conductivity. The presence of Hap in suspension decreases the consistency of polymeric blends probably due to an interaction between Hap and polymers that could change polymer three-dimensional network. The surface tension seemed to be inversely proportional to the consistency of the solution. The Hap increases the conductivity and this seems to be directly related to the increase of HAp concentration. The X-ray diffraction showed that HAp at 0,1% w/w concentration maintained its crystallinity independently of the solvent in which it was dispersed. The polymer solutions were electrospun and it was possible to obtain a randomly collected and 3D tubular aligned scaffolds. The scaffolds were morphologically characterized by SEM, showing that the lower concentration of HAp (0,1%) was characterized by spherical particles present both in water and acid solution. In water the Hap powder presented a fine fraction and few particles having bigger dimensions. In acid solution, Hap particles had greater dimensions and this is probably due to the solubilization of the fine fraction. The nanofibers without HAp were characterized by a regular morphology and smooth surface, while the presence of HAp in F2 and F3 determined nanofibers with a higher roughness and the presence of aggregates probably attributable to HAp nanoparticles. With TEM it was possible to see that the hydroxyapatite particles were included into the nanofiber structure. The presence of HAp into the fibres increases their wettability independently of its concentration.

The mechanical properties were evaluated and the tubular scaffold with 3 mm diameter seems to have the higher values of maximum tensile force. In the hydrated state, the fibres were more fragile then they were in the dry state, while in the dry state they seem to be poorly deformable, compared to the hydrated state. The F3 tubular scaffold with 0,8 mm diameter had a high deformability but a low resistance. The F2 fibres had a higher resistance and deformation, it shows that the presence of HAp at 0,1% w/w concentration gives a greater elasticity and resistance to break, especially when the fibres were electrospun in tubular 3D aligned structure that mimics the structure of the tendon (in dry and hydrated state).

Other studies should be developed (biopharmaceutical characterization) to see if the fibres are biocompatible with cell lines such as human fibroblasts, tenocytes and saos-2, to clarify about the adhesion and the growth of the cells on the fibres, demonstrating that tubular aligned structure allows a better cell adhesion and proliferation. This type of studies has been done over the last few years and the developed systems seems to be promising as tendon substitutes in orthopaedic tissue engineering, as soft tissue engineering. Hopefully it will become as promising as it has been demonstrating with hard tissue engineering.

7 References

1. Frank CBS, Shrive CB, Frank IKY, Hart DA: Form and function of tendon and ligament. In: Einhorn TA, O'Keefe RJ, Buckwalter JA (eds) Orthopaedic basic science, 3rd edn. American Academy of Orthopaedic Surgeons, Rosemont, 2007. pp 199–222
2. Voleti, P. B., Buckley, M. R., & Soslowsky, L. J. Tendon Healing: Repair and Regeneration. Annual Review of Biomedical Engineering,2012. 14(1), 47–71.
3. Kannus, P. Structure of the tendon connective tissue. Scandinavian Journal of Medicine and Science in Sports,2000. 10(6), 312–320
4. Roshan J. MS, G. Kesturu PhD, G. Balian PhD, A. B. Chhabra MD. Tendon: Biology, Biomechanics, Repair, Growth Factors, and Evolving Treatment Options. The Journal of Hand Surgery, 2008. vol. 33 (1), p. 102-112
5. Lomas A. J., Ryan C. N., Sorushanova A., Shologu N., Sideri A. I., Tsioli V, Fthenakis G. C., Tzora A., Skoufos I., Quinlan L. R., O'Laighin G., Mullen A. M., Kelly J. L., Kearns S., Biggs M., Pandit A., Zeugolis D. I. The past, present and future in scaffold-based tendon treatments. Adv Drug Deliv Rev.2015, vol. 84, p. 257-277,
6. Magnusson P., Hansen P., Kjñr M. Tendon properties in relation to muscular activity and physical training. Scand J Med Sci Sports,2003, vol. 13, p. 211-223
7. Tero A.H. Jarvinen, Teppo L.N. Jarvinen, Pekka Kannus, Làszò Jòzsa and Markku Jarvinen. Collagen fibres of the spontaneously ruptured human tendons display decreased thickness and crimp angle. Journal of Orthopaedic Research 2004.22, p. 1303-1309
8. Screen H. R. C., Bader D. L., Lee D. A. Shelton and J. C. Local Strain Measureme nt within Tendon. Strain, 2004. vol. 40, p. 157–163,
9. Sharma P. and Maffulli N. Biology of tendon injury: healing, modeling and remodeling. J Musculoskelet Neuronal Interact, 2006.vol. 6(2), p. 181-190,
10. Fratz P., Misof K., and Zizak I. Fibrillar Structure and Mechanical Properties of Collagen. Journal of Structural Biology; 1997, vol. 122, p. 119-122,
11. Acharya, G. U., Kumar, A., Rajasekar, S., & Samuel, A. J. Reliability and validity of Kannada version of Victorian Institute of Sports Assessment for patellar tendinopathy (VISA-P-K) questionnaire. Journal of Clinical Orthopaedics and Trauma 2018.08.017
12. Hess G.P, Cappiello W.L., Poole R.M., Hunter S.C. Prevention and treatment of overuse tendon injuries. Sports Med. 1989. vol. 8(6), p. 371-84,
13. Walden, G., Liao, X., Donell, S., Raxworthy, M. J., Riley, G. P., & Saeed, A. A Clinical, Biological, and Biomaterials Perspective into Tendon Injuries and Regeneration. Tissue Engineering Part B: Reviews, 2017. 23(1), 44–58.
14. Wang, J. H.-C., & Nirmala, X. Application of Tendon Stem/Progenitor Cells and Platelet-Rich Plasma to Treat Tendon Injuries. Operative Techniques in Orthopaedics, 2016. 26(2), 68–72.
15. O'Brien, F. J. Biomaterials & scaffolds for tissue engineering. Materials Today. 2011., 14(3), 88–95.
16. Verdiyeva G, Koshy K, Glibbery N, Mann H, Seifalian AM. Tendon reconstruction with tissue engineering approach - A review. J Biomed Nanotechnol. 2015;11(9):1495–523.
17. Beachley, V., & Wen, X. Effect of electrospinning parameters on the nanofiber diameter and length. Materials Science and Engineering: C, 2009. 29(3), 663–668.
18. Smith, L. A., & Ma, P. X. Nano-fibrous scaffolds for tissue engineering. Colloids and Surfaces B: Biointerfaces, 2004., 39(3), 125–131.

19. Li, W.-J., Laurencin, C. T., Caterson, E. J., Tuan, R. S., & Ko, F. K. Electrospun nanofibrous structure: A novel scaffold for tissue engineering. Journal of Biomedical Materials Research, 2002. 60(4), 613–621
20. Hinderer, S., Layland, S. L., & Schenke-Layland, K. ECM and ECM-like materials — Biomaterials for applications in regenerative medicine and cancer therapy. Advanced Drug Delivery Reviews, 2016. 97, 260–269.
21. Kumbar, S. G., James, R., Nukavarapu, S. P., & Laurencin, C. T. Electrospun nanofiber scaffolds: engineering soft tissues. Biomedical Materials, 2008. 3(3), 034002.
22. Bhardwaj N., Kundu S.C. Electrospinning: A fascinating fiber fabrication technique. Biotechnology Advances, 2010, vol. 28, p. 325–334
23. Li D, McCann JT, Xia Y, Marquez M. Electrospinning: A simple and versatile technique for producing ceramic nanofibers and nanotubes. Journal of the American Ceramic Society. 2006;89(6):1861 - 1869.
24. Chong EJ, Phan TT, Lim IJ, Zhang YZ, Bay BH, Ramakrishna S, et al. Evaluation of electrospun PCL/gelatin nanofibrous scaffold for wound healing and layered dermal reconstitution. Acta Mater 2007; 3:321–30
25. Mit-uppatham C., Nithitanakul M., Supaphol P. Ultrafine electrospun polyamide-6 fibers: effect of solution conditions on morphology and average fiber diameter. Macromol Chem Phys, 2004. vol. 205, p.2327–38.
26. Casper, C. L., Stephens, J. S., Tassi, N. G., Chase, D. B., & Rabolt, J. F. Controlling Surface Morphology of Electrospun Polystyrene Fibers: Effect of Humidity and Molecular Weight in the Electrospinning Process. Macromolecules, 2004. 37(2), 573–578.
27. Avinash B., Yiu-Wing M., Shing Chung J.W, Mojtaba A., Pei C. Electrospinning of Polymer Nanofibers: Effects on Oriented Morphology, Structures and Tensile Properties. Composites Science and Technology, 2010. vol. 70, p. 703-718.
28. Bharambe S V., Darekar AB, Saudagar RB. Wound healing dressings and drug delivery systems: A review. Int J Pharm Technol 2013;5(3):2764–86.
29. Sahariah P, Másson M. Antimicrobial Chitosan and Chitosan Derivatives: A Review of the Structure-Activity Relationship. Biomacromolecules. 2017; 18(11):3846–68.
30. Tiyaboonchai W. Chitosan Nanoparticles: A Promising System for Drug Delivery. Naresuan Univ J. 2003;11(3):51–66.
31. Francis Suh JK, Matthew HWT. Application of chitosan-based polysaccharide biomaterials in cartilage tissue engineering: A review. Biomaterials. 2000;21(24):2589–98.
32. Rinaudo M. Chitin and chitosan: Properties and applications. Prog Polym Sci. 2006;31(7):603–32.
33. Kean T, Thanou M. Biodegradation, biodistribution and toxicity of chitosan. Adv Drug Deliv Rev [Internet]. 2010;62(1):3–11.
34. Croisier F, Jérôme C. Chitosan-based biomaterials for tissue engineering. Eur Polym J [Internet]. 2013;49(4):780–92.
35. Prajapati, V. D., Jani, G. K., & Khanda, S. M. Pullulan: An exopolysaccharide and its various applications. Carbohydrate Polymers, 2013. 95(1), 540–549.
36. Singh RS, Saini GK, Kennedy JF. Pullulan: Microbial sources, production and applications. Carbohydr Polym. 2008;73(4):515–31.
37. Le Visage, C., Gournay, O., Benguirat, N., Hamidi, S., Chaussumier, L., Mougenot, N., … Norol, F. Mesenchymal Stem Cell Delivery into Rat Infarcted Myocardium Using a Porous Polysaccharide-Based Scaffold: A Quantitative Comparison With Endocardial Injection. Tissue Engineering Part A, 2012. 18(1-2), 35–44.

38. LeGeros RZ. Properties of osteoconductive biomaterials: Calcium phosphates. Clin Orthop Relat Res. 2002;(395):81–98.
39. Alves Cardoso D, Jansen JA, G. Leeuwenburgh SC. Synthesis and application of nanostructured calcium phosphate ceramics for bone regeneration. J Biomed Mater Res Part B Appl Biomater. 2012;100B (8):2316–26.
40. Wahl DA, Czernuszka JT. Collagen-hydroxyapatite composites for hard tissue repair. Eur Cells Mater. 2006; 11:43–56.
41. Rho JY, Kuhn-Spearing L, Zioupos P. Mechanical properties and the hierarchical structure of bone. Med Eng Phys. 1998;20(2):92–102.
42. Wahl DA, Czernuszka JT. Collagen-hydroxyapatite composites for hard tissue repair. Eur Cells Mater. 2006; 11:43–56.
43. Wakai F. Development of Superplastic Ceramics [Internet]. Second Edition. Handbook of Advanced Ceramics: Materials, Applications, Processing, and Properties: Second Edition. Elsevier; 2013. 765–771 p.
44. Nandi SK, Roy S, Mukherjee P, Kundu B, De DK, Basu D. Orthopaedic applications of bone graft & graft substitutes: A review. Indian J Med Res. 2010;132(7):15–30.
45. Kumta PN, Sfeir C, Lee DH, Olton D, Choi D. Nanostructured calcium phosphates for biomedical applications: Novel synthesis and characterization. Acta Biomater. 2005;1(1):65–83.
46. Legeros Z. R. Properties of Osteoconductive Biomaterials: Calcium Phosphates. Clinical Orthopaedics and Related Research, 2002. vol. 395, p. 81-98.
47. Matsunaga K, Murata H, Shitara K. Theoretical calculations of the thermodynamic stability of ionic substitutions in hydroxyapatite under an aqueous solution environment. J Phys Condens Matter. 2010;22(38).
48. Elliott JC. Structure and chemistry of the apatites and other calcium orthophosphates. Amsterdam: Elsevier; 1994
49. Kay M. I., Young R. A., Posner A. S. Crystal structure of hydroxyapatite. Nature, 1964. vol. 204, p. 1050-1052.
50. Shuilin Wua, Xiangmei Liu, Kelvin W.K. Yeung, Changsheng Liu, Xianjin Yang, Biomimeticporous scaffolds for bone tissue engineering, Materials Science and Engineering R 80 1–36, Elsevier. 2014.
51. Hing KA. Bioceramic bone graft substitutes: Influence of porosity and chemistry. Int J Appl Ceram Technol. 2005;2(3):184–99.
52. Superiore S, Anna S. Materiali per ricostruzione del tessuto osseo. 2016;(June).
53. Raeisdasteh Hokmabad V, Davaran S, Ramazani A, Salehi R. Design and fabrication of porous biodegradable scaffolds: a strategy for tissue engineering. J Biomater Sci Polym Ed [Internet]. 2017;28(16):1797–825.
54. LeGeros RZ. Properties of osteoconductive biomaterials: Calcium phosphates. Clin Orthop Relat Res. 2002;(395):81–98.
55. Wei G, Ma PX. Structure and properties of nano-hydroxyapatite/polymer composite scaffolds for bone tissue engineering. Biomaterials. 2004;25(19):4749–57.
56. Tamimi F, Sheikh Z, Barralet J. Dicalcium phosphate cements: Brushite and monetite. Acta Biomater [Internet]. 2012;8(2):474–87
57. Galsin J. S. Defects in crystalline solids. Solid State Physics, An Introduction to Theory, 2019. p. 513-537.
58. Liu F., Jiang X., Bao S., Wang R., Sun B., Zhu M. Effect of hydroxyapatite whisker surface graft polymerization on water sorption, solubility and bioactivity of the dental resin composite. Materials Science and Engineering C 53, 2015. p. 150-155.

59. Boutinguiza M, Pou J, Comesaña R, Lusquiños F, De Carlos A, León B. Biological hydroxyapatite obtained from fish bones. Mater Sci Eng C [Internet]. 2012;32(3):478–86.
60. Bigi A., Foresti E., Gregoriani R., Ripamonti A., Roveri N., Shah J.S. "The role of magnesium on the structure of biological apatite". Calcif Tissue Int,1992. vol. 50, p. 439-444.
61. Kalita SJ, Bhardwaj A, Bhatt HA. Nanocrystalline calcium phosphate ceramics in biomedical engineering. Mater Sci Eng C. 2007;27(3):441–9.
62. Wahl DA, Czernuszka JT. Collagen-hydroxyapatite composites for hard tissue repair. Eur Cells Mater. 2006; 11:43–56.
63. Kulkarni VS, Shaw C. Surfactants, Lipids, and Surface Chemistry. Essent Chem Formul Semisolid Liq Dosages. 2016;5–19
64. Gheisari H, Karamian E, Abdellahi M. A novel hydroxyapatite -Hardystonite nanocomposite ceramic. 2015;41(4):5967–75.
65. Abifarin JK, Obada DO, Dauda ET, Dodoo-Arhin D. Experimental data on the characterization of hydroxyapatite synthesized from biowastes. 2019; 26:104485.